

AMERICAN UNIVERSITY OF BEIRUT

PHYSICALLY BASED MODEL FOR EXTRACTING DUAL
PERMEABILITY PARAMETERS USING NON-NEWTONIAN
FLUIDS

by
CHRISTELLE NABIL BASSET

A thesis
submitted in partial fulfillment of the requirements
for the degree of Master of Engineering
to the Department of Civil and Environmental Engineering
of the Faculty of Engineering and Architecture
at the American University of Beirut





Beirut, Lebanon
September 2018

AMERICAN UNIVERSITY OF BEIRUT

PHYSICALLY BASED MODEL FOR EXTRACTING DUAL
PERMEABILITY PARAMETERS USING NON-NEWTONIAN
FLUIDS

by
CHRISTELLE NABIL BASSET

Approved by:

	[Signature]
[Dr. Majdi Abou Najm, Assistant Professor] [Civil and Environmental Engineering]	Advisor
	[Signature]
[Dr. Georges Saad, Associate Professor] [Civil and Environmental Engineering]	Member of Committee
	[Signature]
[Dr. Ryan Stewart, Assistant Professor] [Plant and Environmental Sciences]	Member of Committee
	[Signature]
[Dr. Scott Hauswirth, Assistant Professor] [Geological Sciences]	Member of Committee

Date of thesis/dissertation defense: [September 12, 2018]

AMERICAN UNIVERSITY OF BEIRUT

THESIS, DISSERTATION, PROJECT RELEASE FORM

Student Name:

_____ Basset _____ Christelle _____ Nabil _____
Last First Middle

Master's Thesis Master's Project Doctoral Dissertation

I authorize the American University of Beirut to: (a) reproduce hard or electronic copies of my thesis, dissertation, or project; (b) include such copies in the archives and digital repositories of the University; and (c) make freely available such copies to third parties for research or educational purposes.

I authorize the American University of Beirut, to: (a) reproduce hard or electronic copies of it; (b) include such copies in the archives and digital repositories of the University; and (c) make freely available such copies to third parties for research or educational purposes
after: **One ---- year from the date of submission of my thesis, dissertation, or project.**
Two ---- years from the date of submission of my thesis, dissertation, or project.
Three ---- years from the date of submission of my thesis, dissertation, or project.

Christelle Basset

Signature

17 September 2018

Date

ACKNOWLEDGMENTS

First, I would like to express my sincere gratitude to my advisor Prof. Majdi Abou Najm for his continued support on my Master's study and related research, for his cooperation, motivation, and great knowledge. His guidance incented me to widen my research and writing of this thesis from several perspectives.

Second, I would like to thank the rest of my thesis committee: Prof. Georges Saad, Prof. Ryan Stewart and Prof. Scott Hauswirth who provided insightful comments and shared their expertise that greatly assisted the research.

My sincere thanks also goes to Miss Acharout Ammar who assisted my experimental work, and to Mr. Helmi El Khatib and Miss Dima Al Hassanieh who gave me access to the laboratory and research facilities. Without their precious support it wouldn't have been possible to conduct my experiment.

I thank my fellow labmates for the sleepless nights we worked together before deadlines, for their feedback, encouragement and of course friendship.

Last but not the least, I would like to thank my family: my parents and my sister for supporting me spiritually throughout my years of study and through the writing of this thesis.

AN ABSTRACT OF THE THESIS OF

Christelle Basset for Master of Engineering
Major: Environmental and Water Resources Engineering

Title: Physically based model for extracting dual-permeability parameters using non-Newtonian fluids

Dual-permeability models simulate flow and transport within soils characterized by preferential (macro) and matrix (micro) pore domains that each possess distinct hydraulic properties. The lack of suitable methods for determining appropriate and physically meaningful model parameters remains the major challenge to applying these models.

Here, we present a method that constrains *dual-permeability* model parameters using experimental saturated flow results from water and a non-Newtonian fluid. We present two sub-models that solve for the effective pore sizes of micropores and macropores, with macropores represented either with cylindrical (for biological pores) or planar (for shrinkage cracks and fissures) pore geometries. The model determines as well the percent contribution (w_i) of the representative macro and micro pores to water flow.

We applied the model to experimental soil samples constructed with capillary tubes describing the macropores, and proved its ability to derive the bimodal pore size distributions in dual-domain soils using only two fluids. As such, we present this method of characterization of dual structures for improved modeling of non-uniform preferential flow and transport in macroporous soils.

CONTENTS

ACKNOWLEDGMENTS.....	iv
AN ABSTRACT OF THE THESIS OF.....	vi
LIST OF ILLUSTRATIONS.....	ix
LIST OF TABLES	xi

Chapter

I.THEORETICAL BACKGROUND	1
A.Introduction.....	1
B.Why Non-Newtonian Fluids?	3
C.ANA Model.....	6
D.Tortuosity.....	7
E.Preferential Flow Models	10
II.THEORY AND METHODS	14
A.Flow Equation in Parallel Plates.....	14
B.Dual-permeability Cases	17
1.Case 1: Circular micropores and linear macropores	17
2.Case 2: Circular micropores and macropores	20
C.Numerical and Analytical Techniques	21
D.Problem Types.....	22
E.Optimizer Panels	24
F.Experimental Validation.....	25

1.Experimental Setup	25
2.Non-Newtonian Fluid.....	27
3.Soil Columns.....	28
4.Dual Pore Structure Calculations	29
III.RESULTS AND DISCUSSION.....	32
A.Model Predictions under Problem Type 1	32
B.Model Predictions under Problem Type 2	33
C.Model Predictions under Problem Type 3	38
D.Summary of results.....	42
IV.CONCLUSION	43
APPENDIX.....	45
A.Detailed Derivations.....	45
B.Experimental Illustrations	48
BIBLIOGRAPHY	50

ILLUSTRATIONS

Figure	Page
1. Velocity profiles for Newtonian and non-Newtonian fluids.....	4
2. Velocity profiles for three Newtonian fluids with different viscosities and their corresponding velocity ratios (a) and three non-Newtonian Cross model viscosity fluids with different K constants and their corresponding velocity ratios (b) (Abou Najm and Atallah, 2016).....	5
3. Conceptual physical models for water flow (Simunek and van Genuchten, 2008) .	11
4. The two abstractions of the pore structure in dual-structured soils	14
5. Coordinate system, notation used in the analysis and parabolic velocity distribution for flow between parallel fixed plates (Munson et al., 2001)	15
6. Proposed ANA-2 Model (1).....	17
7. Proposed ANA-2 Model (2).....	20
8. Flow of Carreau and Cross fluids through straight rigid circular uniform pipes and long thin uniform plane slits within the porous medium	22
9. Matlab Optimizer Interface	25
10. Infiltration Apparatus for Constant Head Experiment.....	27
11. Pore size distribution of each of the three silica sands	30
12. Bimodal pore size distribution in the dual-domain structure built with one capillary tube of 0.75 mm radius along with the #12/20 (a) of tortuosity $T=1.2$, #20/30 (b) of $T=1.2$ and #40/50 (c) of $T=3$. Experimental results highlighted in red representing the porous structure in two points (R_{micro} , w_{micro}) and (R_{macro} , w_{macro}). Similarly, the two simulated radii predicted by the ANA model highlighted in black with the pre-defined set of weights estimated experimentally using the Hagen-Poiseuille equation.....	35
13. Bimodal pore size distribution in the dual-domain structure built with one and two and capillary tubes of 0.75 mm radius with #12/20 (a) and #20/30 (b) silica sand..	37
14. Cumulative pore size distribution of the dual-domain structure built with one capillary tube of 0.75 mm radius with #12/20 (a), #20/30 (b) and #40/50 silica sand. Red circles signifying the experimental averaged micropore radius and corresponding weight (R_{micro} , $\%V_{micro}$) as well as the experimental (actual) macropore radius and its corresponding weight and numbers (R_{macro} , $\%V_{macro}$). Results of the 25 ANA-2 model runs plotted through a wide array of symbols.	39

15. Cumulative pore size distribution of the dual-domain structure built with one and two and capillary tubes of 0.75 mm radius with #12/20 (a) and #20/30 (b) silica sand	40
16. Actual Infiltration Setup for Constant Head Experiment.....	48
17. Different experimental stages.....	49
18. Preparation of xanthan gum fluids.....	49

TABLES

Table	Page
1. Historic summary of tortuosity-porosity relations.....	8
2. Power Law parameters of the two xanthum gum fluids	28
3. Problem-Type 1 Summary	33
4. Problem Type 2 Summary	37
5. Problem-Type 3 Summary	41

CHAPTER I

THEORETICAL BACKGROUND

A. Introduction

Many soils contain complex structures such as fractures, fissures, cracks, and macropores that dissect the soil matrix. These structures form as result of multiscale complex interactions between soil physical and biogeochemical properties, moisture condition, stress level, and biological activity (Abou Najm et al., 2010), and can affect water and solute transport by creating preferential flow (Beven, 1991). During preferential flow events, non-equilibrium conditions lead to differences in water pressures and solute concentrations (Gerke and van Genuchten, 1993, Jarvis, 2007). Such features of preferential flow cannot be captured by the Richards equation based on the single-porosity approach (Beven and Germann, 1982; van Ghenuchten et al., 1990).

Different approaches have been proposed to describe water flow in the porous media using double-porosity or dual-permeability models (Gerke and van Genuchten, 1993; Jarvis, 1994; Simunek et al., 2003; Lewandowska et al., 2004). The term dual-permeability is used to characterize a porous medium composed of two subdomains with distinct pore sizes and hydraulic conductivities. For example, Gerke and van Genuchten (1993) derived two Richards' equations coupled by an exchange term to represent the water transfer between macropores in a fracture network and micropores in the soil matrix. The exchange term is proportional to the conductivity of the interface and the difference in pressure head between the two domains. Jarvis (1994) described flow in high-permeability domain by kinematic wave equation and assumed the water transfer to be proportional to the

difference in relative saturations. Lewandowska et al. (2004) described flow within each domain using the Richards equation, yet their solution requires knowledge of geometry and hydraulic conductivity of the high-permeability domain.

A major challenge to using these theoretical models is that we currently have limited ability to measure or identify their required parameters (Kohne et al., 2002), especially since inverse identification of macroscopic parameters can encounter several challenges mainly related to the instability and nonuniqueness of the parameters (Larsson and Jarvis, 1999). Non-Newtonian fluids have recently been used to characterize soil properties (Di Federico et al., 2010; Comba et al., 2011; Bush et al., 2014; Gastone et al., 2014; Tosco et al., 2014; Stewart et al., 2014), with Abou Najm and Atallah (2016) building a system of equations that abstracts the pore structure into a system of N pore groups, each having a corresponding representative pore radius (R_i) and percent contribution to water flow (w_i). The model (hereafter referred to as ANA model) requires only the experimental results of saturated flow experiments of the tested medium with water and $N-1$ non-Newtonian fluids. The model was tested on synthetic porous media and demonstrated its ability to extract multiple porosity-permeability domains (Atallah and Abou Najm, 2018).

Here, we use the ANA model with water and a non-Newtonian fluid in saturated flow experiments to extract the physically-based parameters of dual-permeability model required for improved flow predictions. Two sub-models are established to determine the effective macropore sizes assuming either cylindrical or planar pore geometries, with micropores represented by cylindrical geometry. This model also determines the percent contribution to flow (w_i) corresponding to the representative macro and micro pores. A

user-friendly solver was developed to solve the system of equations, including numerical and analytical integration of the non-Newtonian viscosity models.

B. Why Non-Newtonian Fluids?

Non-Newtonian fluids have viscosities that vary with the rate of applied stresses. Their behavior opened a wide range of applications in porous media, including hydraulic fracturing, the injection and delivery of iron particles for soil, and groundwater remediation (Comba et al., 2011; Bush et al., 2014; Gastone et al., 2014; Tosco et al., 2014).

Furthermore, non-Newtonian fluids, used separately or in combination with Newtonian fluids with constant viscosities, proved helpful in aiding the understanding of flow and transport mechanisms in porous media. They were used to characterize the pore space, in terms of flow and porosity (Di Federico et al., 2010; Stewart et al., 2014; Abou Najm and Atallah, 2016). Modeling flow of non-Newtonian fluids requires the characterization of fluid's viscosity model before solving the flow equation on the modeled pore structure.

Common viscosity models for non-Newtonian fluids are defined as follows:

$$\text{Power Law} \quad \eta = k \left(-\frac{\partial v_z}{\partial r} \right)^{\alpha-1} \quad (1)$$

$$\text{Cross} \quad \eta = \eta_\infty + \frac{\eta_0 - \eta_\infty}{1 + k \left(-\frac{\partial v_z}{\partial r} \right)^{1-\alpha}} \quad (2)$$

$$\text{Carreau-Yasuda} \quad \eta = \eta_\infty + \frac{\eta_0 - \eta_\infty}{\left[1 + \left(-k \frac{\partial v_z}{\partial r} \right)^\lambda \right]^{\frac{1-\alpha}{\lambda}}} \quad (3)$$

$$\text{Carreau} \quad \eta = \eta_\infty + \frac{\eta_0 - \eta_\infty}{\left[1 + \left(-k \frac{\partial v_z}{\partial r} \right)^2 \right]^{\frac{1-\alpha}{2}}} \quad (4)$$

where k is the consistency index or the viscosity at a shear rate of 1 s^{-1} [$\text{M L}^{-1} \text{ T}^{-1}$], α the exponent in dimensionless units (1 for Newtonian, $0 < \alpha < 1$ for shear thinning, and $\alpha > 1$ for shear thickening fluids), η_0 the viscosity at zero shear rate [$\text{M L}^{-1} \text{ T}^{-1}$], η_∞ the viscosity at infinite shear rate [$\text{M L}^{-1} \text{ T}^{-1}$] and λ the relaxation time [T].

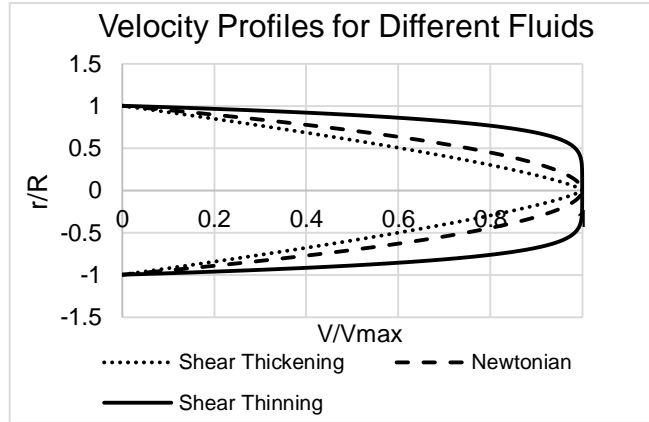
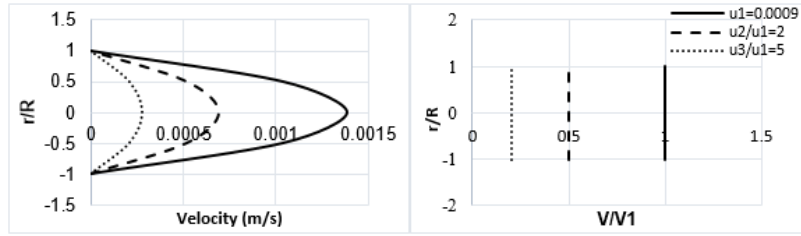


Figure 1: Velocity profiles for Newtonian and non-Newtonian fluids

Figure 1 presents three different velocity profiles depending on the fluid behavior, representing three of the most common flow patterns (Newtonian, and non-Newtonian shear thinning and thickening). Here we analyze the cross-sectional flow of non-Newtonian fluid and we compare it with the Newtonian's flow. For Newtonian fluid, the structure of the flow is quadratic ($V \propto r^2$ from Poiseuille Law). For shear thinning fluid, the velocity profile is flatter near the boundary of the cross-sectional pipe (i.e. lower viscosity), then it reaches its maximum V_{max} at the middle covering a wider range of the cross-section. For shear thickening fluid, the velocity profile is steeper near the boundary walls (i.e. higher viscosity), then it decays faster towards the middle to reach V_{max} exactly at the midpoint of the cross-sectional area.

Newtonian Fluid Behavior (a)



Non-Newtonian Fluid Behavior - Cross Model (b)

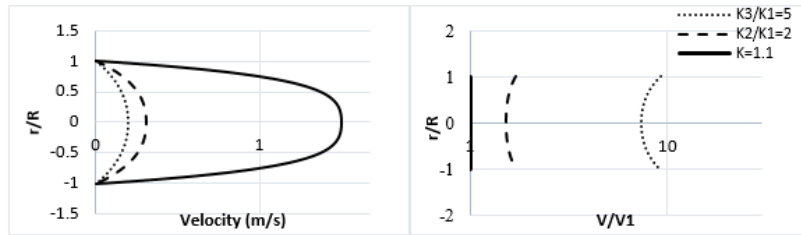


Figure 2: Velocity profiles for three Newtonian fluids with different viscosities and their corresponding velocity ratios (a) and three non-Newtonian Cross model viscosity fluids with different K constants and their corresponding velocity ratios (b) (Abou Najm and Atallah, 2016)

Figure 2 (a) shows that using three Newtonian fluids with three different viscosities did not generate additional unique information related to flow. This explains the reason why using more than one Newtonian fluid on the same porous medium generates flows that are proportional to the inverse of their corresponding viscosities. On the other hand, flow ratios from the three different non-Newtonian fluids generated additional unique information which can be used in porosity characterization. The flows within the same porous medium are proportional to different powers of the pore structure, thus presenting additional unique information that can be used in the characterization of different pore structures (Figure 2 (b)). From that point, Abou Najm and Atallah (2016) proved that

combining water and N - I non-Newtonian fluids can result in N unique flow signatures for each pore size.

C. ANA Model

Abou Najm and Atallah (2016) utilized water and N - I non-Newtonian fluids on saturated soil samples to represent the pore structure with N radii, such that each radius has a corresponding contribution to total water flow.

Assuming steady-state, incompressible, saturated and laminar flow under isothermal conditions having a generalized Newtonian viscosity models, the Navier-Stokes equations for flow in circular in cylindrical coordinates reduce as follows to:

$$\frac{1}{r} \frac{d}{dr} \left(r \eta \frac{dv_z}{dr} \right) = \rho g \frac{\left(\frac{\partial h}{\partial z} - 1 \right)}{T} \quad (5)$$

where: ρ is the density [$M L^{-3}$], g is the gravitational acceleration [$M T^{-2}$], η is the dynamic viscosity [$M L^{-1} T^{-1}$], and $\frac{\partial v_z}{\partial r}$ is the shear rate [$L T^{-1}$] and $\frac{\partial h}{\partial z}$ is the head gradient per unit length [$L L^{-1}$], and T is the tortuosity factor [$L L^{-1}$]. For horizontal flow, the right hand side of the governing differential equation becomes equal to: $\rho g \frac{\left(\frac{\partial h}{\partial z} \right)}{T}$.

A $N \times N$ square matrix is derived by associating two systems. The first system is flow generated from N constant head experiments (using water and N - I non-Newtonian fluids) on real soil and the second system is the flow from N representative effective radii along with their corresponding weights. In addition, the last row of the matrix is derived by equating the pore volume of the real soil to the volume of the representative system as follows:

$$\underbrace{\begin{bmatrix} \frac{[2\pi \int_0^{R_1} r \times v^{S_2} dr]}{R_1^4} & \frac{[2\pi \int_0^{R_2} r \times v^{S_2} dr]}{R_2^4} & \frac{[2\pi \int_0^{R_3} r \times v^{S_2} dr]}{R_3^4} & \dots & \frac{[2\pi \int_0^{R_N} r \times v^{S_2} dr]}{R_N^4} \\ \frac{[2\pi \int_0^{R_1} r \times v^{S_3} dr]}{R_1^4} & \frac{[2\pi \int_0^{R_2} r \times v^{S_3} dr]}{R_2^4} & \frac{[2\pi \int_0^{R_3} r \times v^{S_3} dr]}{R_3^4} & \dots & \frac{[2\pi \int_0^{R_N} r \times v^{S_3} dr]}{R_N^4} \\ \vdots & \vdots & \vdots & \ddots & \vdots \\ \frac{[2\pi \int_0^{R_1} r \times v^{S_N} dr]}{R_1^4} & \frac{[2\pi \int_0^{R_2} r \times v^{S_N} dr]}{R_2^4} & \frac{[2\pi \int_0^{R_3} r \times v^{S_N} dr]}{R_3^4} & \dots & \frac{[2\pi \int_0^{R_N} r \times v^{S_N} dr]}{R_N^4} \\ T_1 \frac{[2\pi \int_0^{R_1} r \times 1 dr]}{R_1^4} & T_2 \frac{[2\pi \int_0^{R_2} r \times 1 dr]}{R_2^4} & T_3 \frac{[2\pi \int_0^{R_3} r \times 1 dr]}{R_3^4} & \dots & T_N \frac{[2\pi \int_0^{R_N} r \times 1 dr]}{R_N^4} \end{bmatrix}}_A \underbrace{\begin{bmatrix} w_1 T_1 \\ w_2 T_2 \\ w_3 T_3 \\ \vdots \\ w_N T_N \end{bmatrix}}_w = \underbrace{\begin{bmatrix} \frac{Q_2 C_1}{Q_1} \\ \frac{Q_3 C_1}{Q_1} \\ \vdots \\ \frac{Q_N C_1}{Q_1} \\ \frac{\phi A_T C_1}{Q_1} \end{bmatrix}}_B \quad (6)$$

where: R_i is the representative radius [L], v_{S_j} is the velocity function for fluid S_j [$L T^{-1}$], w_i is the flow contribution of each radius R_i , Q_j is the flow generated from the j^{th} infiltration experiment [$L^3 T^{-1}$], ϕ is the porosity of the porous media [$L^3 L^{-3}$], A_T is the total area of the porous media [L^2], and $C_1 = \pi \frac{\alpha}{1+3\alpha} \left[-\frac{H}{2\beta} \right]^{\frac{1}{\alpha}}$ (with β as the consistency index in [$M L^{-1} T^{-1}$], α is the exponent in dimensionless units, with $\alpha = 1$ for water, and $H = \rho g \left(\frac{\partial h}{\partial z} - 1 \right)$ for vertical flow or $\rho g \frac{\partial h}{\partial z}$ for horizontal flow).

As a simplistic approach, Abou Najm and Atallah (2016) solve the proposed model of N parallel capillary tubes assuming tortuosity is equal to 1. However, water flow is sensitive to the changes in tortuosity within the soil structure. The infiltration rate of water is slow due to tortuosity, the extent to which pathways are winding rather than straight or direct. Thus, tortuosity should be considered as a model parameter for characterization of porous dual structures.

D. Tortuosity

The soil structure is a complex and highly interconnected network of three-dimensional pores. Representing such complexities with dual structures or one dimensional

bundles of capillary tubes may be practical for some soil applications but surely does not satisfy all soil structures. To account for some of the structural complexities that are beyond the capabilities of the simple model of parallel tubes, tortuosity was incorporated in the model with the ability to put different tortuosities for each of the dual structures. Tortuosity is defined as the ratio of the actual distance traveled by a fluid through the pore structure (l_e) to the straight line distance (l) crossing the porous medium, i.e. $T = \frac{l_e}{l}$ (Moldrup et al., 2001). It is commonly characterized by the porosity of the porous medium with typical range between 1.2 and 3, but can reach values as high as 50 for low porosity media (Matyka et al., 2008). However, Carey et al. (2016) indicated that total porosity is a poor predictor for tortuosity coefficient, and suggested hydraulic conductivity as more reliable predictor for tortuosity. A comprehensive summary of different theoretical and experimental attempts to define tortuosity is summarized in Table 1.

Table 1: Historic summary of tortuosity-porosity relations

Reference	Relation	Type of soil	Method of Analysis	Type of Tortuosity
Maxwell (1881)	$T = 1.5 - 0.5\phi$	Ordered packing	Theoretical	Electric
Bruggeman (1935)	$T = \phi^{-0.5}$	Non mono-sized spheres	Theoretical	Electric
Carman (1937)	$T = 2$	Equal-sized spheres	Theoretical	Hydraulic
Archie (1942)	$T = \phi^{-0.4}$	Consolidated sandstones $0.1 < \phi < 0.6$	Empirical	Electric
Millington and Quirk (1961)	$T = \phi^{-1/3}$	Partly saturated homogeneous isotropic mono-disperse spheres	Theoretical	Diffusive
Weissberg (1963)	$T = 1 - 0.5\ln(\phi)$	Bed of overlapping spheres	Empirical	Diffusive
Dullien (1975)	$T = 3$	Parallel capillary model	Theoretical	Hydraulic

Berryman (1981)	$T = (1 + 1/\phi)/2$	Fully consolidated granular constituents	Theoretical	Hydraulic
Beekman (1990)	$T = \frac{\phi}{1 - (1 - \phi)^{1/3}}$	Heterogeneous $0.1 < \phi < 0.7$	Theoretical	Diffusive
Du Plessis and Masliyah (1991)	$T = \frac{\phi}{1 - (1 - \phi)^{2/3}}$	Isotropic granular media	Analytical	Hydraulic
Boudreau (1996)	$T = \sqrt{1 - \ln(\phi^2)}$	Fine-grained unlithified sediments $\phi < 0.85$	Empirical	Diffusive
Mauret and Renaud (1997)	$T = 1 - 0.49\ln(\phi)$	Packed beds with spherical particles	Experimental	Hydraulic
Boving and Grathwohl (2001)	$T = \phi^{-1.2}$	Limestone and sandstone rocks $\phi > 0.2$	Experimental	Diffusive
Mota et al. (2001)	$T = \phi^{-0.4}$	Spherical particles	Empirical	Hydraulic
Yu and Li (2004)	$T = \frac{1}{2} \left[1 + \frac{\alpha}{2} + \alpha \frac{\sqrt{\left(\frac{1}{\alpha} - 1\right)^2 + \frac{1}{4}}}{1 - \alpha} \right]$ where $\alpha = \sqrt{1 - \phi}$	Square particles	Theoretical	Geometric
Yun et al. (2005)	$T = \frac{T_1^* + T_2^{**}}{2}$	Spherical overlapping particles	Theoretical	Geometric
Matyka et al. (2008)	$T = 1 - 0.77\ln(\phi)$	Overlapping mono-sized squares $\phi \geq 0.4$	Empirical	Hydraulic
Lanfrey et al. (2010)	$T = 1.23 \frac{(1 - \phi)^{4/3}}{S^2 \phi}$ where S: sphericity factor	Bed of spheres	Theoretical	Geometric
Ahmadi et al. (2011)	$T = \sqrt{\frac{2\phi}{3[1 - 1.209(1 - \phi)^{2/3}]} + \frac{1}{3}}$	Mono-sized spherical particles $\phi \geq 0.3$	Theoretical	Hydraulic
Duda et al. (2011)	$T = 1 + (1 - \phi)^{1/2}$	Freely overlapping squares $\phi < 0.8$	Empirical	Hydraulic
Pisani (2011)	$T = \frac{1}{1 - S(1 - \phi)}$ where S: sphericity factor	Random, partial overlapping shapes	Theoretical	Diffusive

Li and Yu (2011)	$T = \left(\frac{19}{18}\right)^{\ln(\phi)/\ln(8/9)}$	Particles of same size	Analytical	Geometric
Liu and Kitanidis (2013)	$T = \phi^{0.28} + 0.15$	Isotropic spherical grains $0.25 < \phi < 0.5$	Empirical	Electric
Saomoto and Katagiri (2015)	$T = 1 + 0.217(\phi^{-1.748} - 1)^{0.428}$	Packed beds with spherical particles $0.5 \leq \phi \leq 0.9$	Empirical	Hydraulic
Carey et al. (2016)	$T = \sqrt{1/(0.77K^{0.04})}$	Saturated unconsolidated soil $0.3 \leq \phi \leq 0.5$	Experimental	Diffusive

$$* T_1 = \frac{\left[1 + \frac{\sqrt{3}(\pi-2)}{6+3P}\right] + \left[\frac{\sqrt{2+3P^2/4+3P} + \arccos(\sqrt{3}(2+P)/2)^{-1}}{\sqrt{3}(2+P)/2}\right]}{4} + \frac{\frac{1}{\sqrt{1-\left[\frac{1}{\sqrt{3}(2+P)/2}\right]^2}} + \frac{1}{\sqrt{1-\left[\frac{1}{\sqrt{3}(2+P)/2-1}\right]^2}}}{4}$$

$$** T_2 = \left(1 - \frac{P_1}{P_1+1}\right) \left(1 + \frac{\pi-2}{P_1+2}\right) + \frac{P_1}{P_1+1}, \quad P = \sqrt{2\pi/(\sqrt{3}(1-\phi))} \quad \text{and} \quad P_1 = \sqrt{\pi/(1-\phi)} - 2$$

E. Preferential Flow Models

At this point, we introduce the past common modeling approaches of preferential flow with their limitations that triggered us to develop a physically based dual-permeability model using the ANA model for improved characterization of dual structures.

Preferential flow has been described by wide range of modeling approaches, most commonly using dual structures, namely dual-porosity models (van Genuchten and Wierenga, 1976) and dual-permeability models (Gerke and van Genuchten, 1993; Jarvis, 1994; Simunek et al., 2003; Lewandowska et al., 2004). Both models divide the porous medium into two sub-regions, one characterized by the macropore network (fracture, inter-porosity domain) and one by the micropore network (matrix, intra-porosity domain). Compared to single pore domain models, dual-domain models involve additional parameters that describe the dual pore regions.

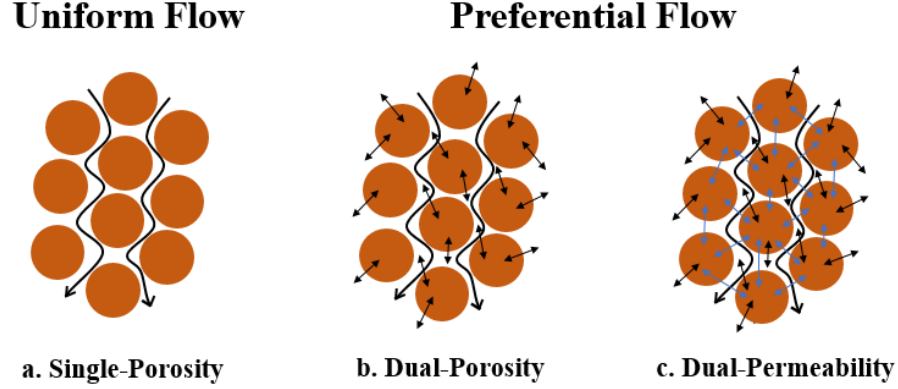


Figure 3: Conceptual physical models for water flow (Simunek and van Genuchten, 2008)

Dual-porosity models (Figure 3 (b)) assume that water is immobile between the micropores, such that water can move from the macropore into the soil aggregates and vice versa, but not directly between the aggregates themselves. For that reason, water is considered immobile in the aggregates from a larger scale. The dual-porosity formulation for water flow describes water flow in the macropores (subscript mo for mobile region) using the Richards Equation and the moisture dynamics in the matrix (subscript im for immobile region) using a mass balance equation (Simunek et al., 2003):

$$\frac{\partial \theta_{mo}(h_{mo})}{\partial t} = \frac{\partial}{\partial z} \left[K(h_{mo}) \left(\frac{\partial h_{mo}}{\partial z} + 1 \right) \right] - S_{mo}(h_{mo}) - \tau_w \quad (7)$$

$$\frac{\partial \theta_{im}(h_{im})}{\partial t} = -S_{im}(h_{im}) + \tau_w \quad (8)$$

where $z[L]$ the vertical coordinate (positive in the upward direction), $t [T]$ time, $h[L]$ the pressure head, $\theta(h)$ the soil water retention curve describing the relationship between the water content $\theta[L^3L^{-3}]$ and the pressure head $h[L]$, $K(h)$ the unsaturated hydraulic conductivity (often equal to the product of the relative hydraulic conductivity $K_r(\text{dimensionless})$ and the saturated hydraulic conductivity $K_s(LT^{-1})$), $S(T^{-1})$ a sink

term describing the root water uptake, and $\tau_w(T^{-1})$ the water transfer between the two pore regions.

However, dual-permeability models overcome the limitation of water being immobile between aggregates. In such models (Figure 3 (c)), the porous medium consists of two homogeneous regions, one associated with the macropore (fracture, inter-porosity domain) of high permeability, and the other associated with the micropore (matrix, intra-porosity domain) of low permeability. This concept was used in the model proposed by Gerke and van Genuchten (1993) that consists of two Richards' equations coupled by an exchange term to represent the water transfer between the two pore regions. The flow equations for the macropore (subscript f for fracture) and micropore (subscript m for matrix) are given by:

$$\frac{\partial \theta_f(h_f)}{\partial t} = \frac{\partial}{\partial z} \left[K_f(h_f) \left(\frac{\partial h_f}{\partial z} + 1 \right) \right] - S_f(h_f) - \frac{\tau_w}{\omega} \quad (9)$$

And

$$\frac{\partial \theta_m(h_m)}{\partial t} = \frac{\partial}{\partial z} \left[K_m(h_m) \left(\frac{\partial h_m}{\partial z} + 1 \right) \right] - S_m(h_m) - \frac{\tau_w}{1-\omega} \quad (10)$$

Respectively, where, ω (*dimensionless*) the ratio of the volume of the macropore domain to the volume of the total soil domain.

The water transfer $\tau_w(T^{-1})$ between the two pore regions is described as follows:

$$\tau_w = \alpha_w (h_f - h_m) \quad (11)$$

where $h_f(L)$ and $h_m(L)$ the average pressure potentials in the macropores and in the micropores respectively, and $\alpha_w(L^{-1}T^{-1})$ a first-order coefficient defined as follows:

$$\alpha_w = \frac{\beta}{a^2} \gamma_w K_a \quad (12)$$

where β a geometry factor ($\beta = 3$ for rectangular aggregates and $\beta = 15$ for spherical aggregates), a [L] the distance from the center of a matrix block to the fracture boundary, γ_w an empirical coefficient assumed as 0.4 and K_a the apparent hydraulic conductivity defined as : $K_a = 0.5[K_a(h_f) + K_a(h_m)]$.

Those theoretical models are still limited because they require parameters that cannot be directly identified (Kohne et al., 2002). The inverse identification of the macroscopic parameters can encounter challenges since the sources of errors cannot be distinguished during the analysis like model or parameters errors (Larsson and Jarvis, 1999). Therefore, it is very difficult to use those models under field conditions, due to the large number of parameters involved and the current lack of standard experimental procedures to estimate them. For that reason, a new physically based dual-permeability model should be presented to overcome the current inabilities of the earlier flow models to cope with the complexities of the pore medium.

CHAPTER II

THEORY AND METHODS

In this work, we use the ANA model to develop a 2x2 matrix (solving for the case of $N = 2$) that can be used to extract physically based dual-permeability model parameters. We refer to this model as ANA-2 model. We simplify the pore structure into one of two configurations (Figure 4): micropores represented by cylindrical pore geometries with macropores either in cylindrical (e.g., biological pores) or planar (e.g., shrinkage cracks and fissures) pore geometries.

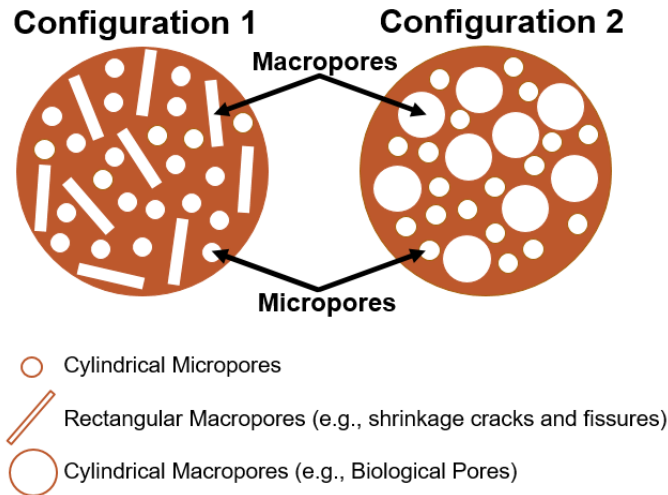


Figure 4: The two abstractions of the pore structure in dual-structured soils

A. Flow Equation in Parallel Plates

Given that macropores can attain planar and cylindrical pore geometries, we re-derive the ANA model for the case when part of the pore structure is represented as

rectangular sections (macropores) by using the solutions of flow with parallel plates' conditions.

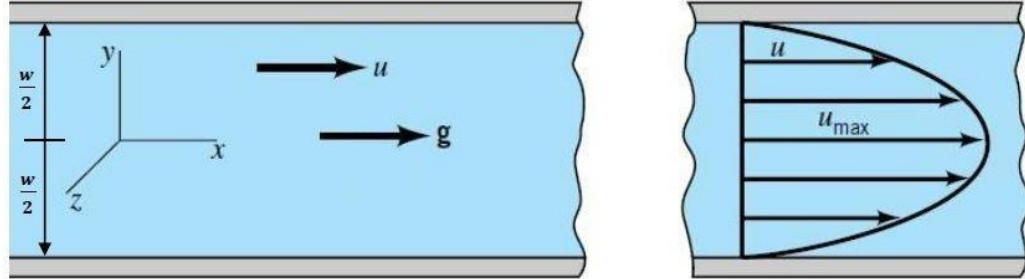


Figure 5: Coordinate system, notation used in the analysis and parabolic velocity distribution for flow between parallel fixed plates (Munson et al., 2001)

Assuming steady-state, incompressible, saturated and laminar flow under isothermal conditions having a generalized Newtonian viscosity models, the Navier-Stokes equations for flow between fixed parallel plates in Cartesian coordinates reduce as follows to:

$$\frac{d}{dy} \left(n \frac{du}{dy} \right) = \frac{dP}{dx} - \rho g \quad (13)$$

where P is the pressure, ρ is the density ($M L^{-3}$), g is the gravitational acceleration ($M T^{-2}$), n is the dynamic viscosity in ($P T$) and $\frac{du}{dy}$ is the shear rate in (T^{-1}). Assuming a constant pressure gradient:

$$\frac{d}{dy} \left(n \frac{du}{dy} \right) = \rho g \left(\frac{dh}{dx} - 1 \right) = H \quad (14)$$

where $\frac{dh}{dx}$ is the pressure head gradient per unit length, while H is the overall hydraulic head term for vertical flow. For horizontal flow, H becomes $\rho g \left(\frac{dh}{dx} \right)$.

To account for tortuosity:

$$\frac{d}{dy} \left(n \frac{du}{dy} \right) = \frac{H}{T} \quad (15)$$

where T is the tortuosity factor

Assuming **power law viscosity model** fluids with different α constants,

$$n = \beta \left(-\frac{du}{dy} \right)^{\alpha-1} \quad (16)$$

where β is the consistency index in (P T) or the viscosity at a shear rate of 1s^{-1} , α is the exponent in dimensionless units (1 for Newtonian, $0 < \alpha < 1$ for shear thinning, > 1 for shear thickening).

The velocity profile derived in the special case of non-Newtonian power law viscosity model is as follows (detailed derivations are provided in the Appendix).

$$u = \frac{\alpha}{\alpha+1} \left(-\frac{H_j}{\beta} \frac{1}{T_i} \right)^{\frac{1}{\alpha}} \left\{ \frac{1}{2^{\frac{1}{\alpha}+1}} W^{\frac{1}{\alpha}+1} - y^{\frac{1}{\alpha}+1} \right\} \quad (17)$$

where W (L) is the distance between the two parallel fixed plates as shown in Figure 5

The general flow equation is then derived by integrating u using the general flow equation for parallel fixed plates:

$$q = \int_{-W/2}^{W/2} u dy \quad (18)$$

The analytical equation of flow through parallel plates in the special case of non-Newtonian power law viscosity model is therefore:

$$Q = \frac{\alpha}{(2\alpha+1)2^{\frac{1}{\alpha}+1}} \left(-\frac{H_j}{\beta} \frac{1}{T_i} \right)^{\frac{1}{\alpha}} b W^{\frac{1}{\alpha}+2} \quad (19)$$

where b (L) is the width of the plane normal to the plane shown in Figure 5

B. Dual-permeability Cases

As it has been already mentioned, this research focuses on improved characterization of dual structures using non-Newtonian fluids. The ANA-2 model assumes two pore configurations: (1) macropores are represented as linear cracks while micropores are represented as circular pores and (2) both micro and macro pores are represented as circular pores.

1. Case 1: Circular micropores and linear macropores

$$Q_j = Q_{jk} + Q_{ji} \quad (20)$$

where j the number of fluids, i the number of linear (i.e. rectangular) macropores and k the number of circular micropores. In case 1, $j = 2$ and $i = k = 1$

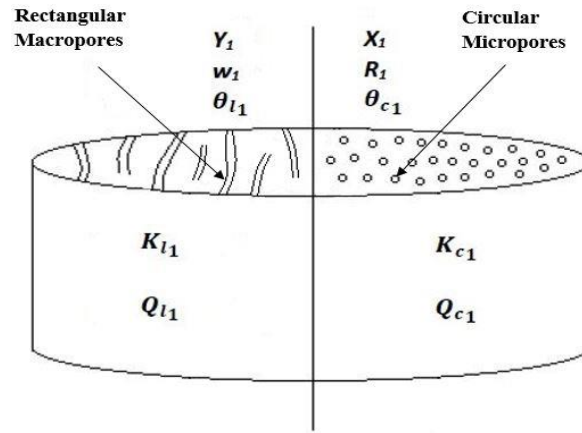


Figure 6: Proposed ANA-2 Model (1)

The pore structure of the porous medium is abstracted into 1 representative radius (R_1) with X_1 the number of circular pores for radius (R_1) and into 1 width (W_1) and length (b_1) with Y_1 the number of linear pores for width (W_1) and length (b_1).

Two equations can be derived from equating the total flow from each of the two solutions (water and one non-Newtonian fluid) to the flow in the proposed pore structure.

The total saturated flow (Q_j) resulting from water in a porous medium idealized into one representative radius (R_1), width (W_1) and length (b_1):

$$Q_1 = A_1 \frac{X_1}{T_{c_1}} R_1^4 + B_1 \frac{Y_1}{T_{l_1}} b_1 W_1^3 \quad (21)$$

$$\text{where: } \begin{cases} A_1 = \frac{\pi}{4} \left[-\frac{H_{c_1}}{2\mu} \right] \\ B_1 = \frac{1}{6} \left[-\frac{H_{l_1}}{2\mu} \right] \\ X_1: \text{number of circular pores for radius } (R_1) \\ Y_1: \text{number of linear pores for width } (W_1) \text{ and length } (b_1) \end{cases}$$

For $j = 2$, the total saturated flow (Q_j) resulting from solution (fluid) S_j in a porous medium idealized into 1 representative radius (R_1), width (W_1) and length (b_1):

$$Q_j = X_1 \left(2\pi \int_0^{R_1} (u_c)^{S_j} r dr \right) + Y_1 \left(2 \int_0^{W_1/2} (u_l)^{S_j} b_1 dy \right) \quad (22)$$

where u_c the velocity in circular pores and u_l the velocity of in linear pores

The total volume of pores within the sample (V_{pores}) can be calculated as:

$$\emptyset V_{pores} = X_1 L_{c_1} \pi R_1^2 + Y_1 L_{l_1} b W_1 \quad (23)$$

where \emptyset the total porosity of the medium sample, V_T the total volume of the sample, L_{c_1} the length of the tube corresponding to R_1 and L_{l_1} the length of the rectangular pores corresponding to width W_1 and length b_1 . Dividing by the sample length L , and using the identities that $L_{c_1} = T_{c_1} L$ and $L_{l_1} = T_{l_1} L$:

$$\emptyset A_T = X_1 T_{c_1} \pi R_1^2 + Y_1 T_{l_1} b_1 W_1 \quad (24)$$

where A_T the total cross-sectional area of the sample, T_{c_1} the tortuosity of the tube corresponding to R_1 and T_{l_1} the tortuosity of the parallel plates corresponding to W_1 and b_1 .

The set of equations is: ($j = 2$)

$$\begin{cases} Q_1 = A_1 \frac{X_1}{T_{c1}} R_1^4 + B_1 \frac{Y_1}{T_{l1}} b_1 W_1^3 \\ Q_2 = X_1 \left(2\pi \int_0^{R_1} (u_c)^{S_2} r dr \right) + Y_1 \left(2 \int_0^{W_1/2} (u_l)^{S_2} b_1 dy \right) \\ \phi A_T = X_1 T_{c1} (\pi R_1^2) + Y_1 T_{l1} b_1 W_1 \end{cases} \quad (25)$$

Dividing the total flow into flow in macropores $[(w_1)_c Q_1]$ vs. flow in micropores $[(w_1)_l Q_1]$: where $(w_1)_c$ the ratio of flow in circular micropores to the total is flow and $(w_1)_l$ the ratio of flow in rectangular macropores to the total flow.

$$\begin{cases} (w_1)_c Q_1 = A_1 \frac{X_1}{T_{c1}} R_1^4 \\ (w_1)_l Q_1 = B_1 \frac{Y_1}{T_{l1}} b_1 W_1^3 \end{cases} \rightarrow \begin{cases} Q_1 = \frac{A_1 X_1 R_1^4}{T_{c1} (w_1)_c} \\ Q_1 = \frac{B_1 Y_1 b_1 W_1^3}{T_{l1} (w_1)_l} \end{cases} \quad (26)$$

$$\text{Subject to } \begin{cases} (w_1)_c + (w_1)_l = 1 \\ w_{min} \leq (w_1)_c \leq 1 \\ w_{min} \leq (w_1)_l \leq 1 \end{cases}$$

Dividing the equations (22) and (24) by Q_1 from (26), we obtain:

$$\underbrace{\begin{bmatrix} \left(\frac{1}{A_1}\right) \frac{(2\pi \int_0^{R_1} (u_c)^{S_2} r dr)}{R_1^4} & \left(\frac{1}{B_1}\right) \frac{(2 \int_0^{W_1/2} (u_l)^{S_2} dy)}{W_1^3} \\ \left(\frac{1}{A_1}\right) \left(T_{c1} \frac{\pi}{R_1^2}\right) & \left(\frac{1}{B_1}\right) \left(T_{l1} \frac{1}{W_1^2}\right) \end{bmatrix}}_{A_1} \underbrace{\begin{bmatrix} T_{c1} (w_1)_c \\ T_{l1} (w_1)_l \end{bmatrix}}_w = \begin{bmatrix} \frac{Q_2}{Q_1} \\ \frac{\phi A_T}{Q_1} \end{bmatrix} \quad (27)$$

A_1 is a matrix derived by incorporating two systems. The first system is the flow generated from 2 constant head experiments (water and 1 non-Newtonian fluid) on the soil and the second system is the flow through micropores represented by a single effective radius R_1 and macropores represented by a single effective width R_1 as well as their corresponding contributions to water flow $(w_1)_c$ and $(w_1)_l$.

2. Case 2: Circular micropores and macropores

$$Q_j = Q_{jk} \quad (28)$$

where j the number of fluids and k the number of circular pores. In case 2, $j = 2$ and $k = 2$

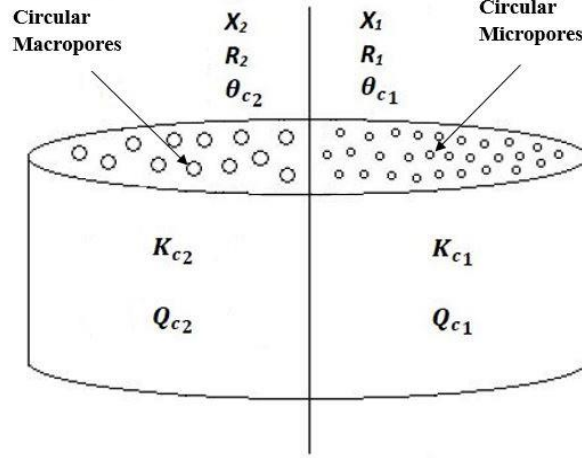


Figure 7: Proposed ANA-2 Model (2)

In the case 2, the model is derived using the same methodology followed in case 1;

$$\underbrace{\begin{bmatrix} \frac{(2\pi \int_0^{R_1} (u_c) S_2 r dr)}{R_1^4} & \frac{(2\pi \int_0^{R_2} (u_c) S_2 r dr)}{R_2^4} \\ \left(T_{c1} \frac{\pi}{R_1^2}\right) & \left(T_{c2} \frac{\pi}{R_2^2}\right) \end{bmatrix}}_{A_2} \underbrace{\begin{bmatrix} T_{c1} (w_1)_c \\ T_{c2} (w_2)_c \end{bmatrix}}_w = \begin{bmatrix} \frac{Q_2 A_1}{Q_1} \\ \frac{\phi A_T A_1}{Q_1} \end{bmatrix} \quad (29)$$

A_2 is a matrix derived by incorporating two systems. The first system is flow generated from two constant head experiments (water and one non-Newtonian fluid) on the soil and the second system is the flow through circular micropores and macropores represented respectively by effective radii R_1 and R_2 as well as their respective corresponding contributions to water flow $(w_1)_c$ and $(w_2)_c$.

C. Numerical and Analytical Techniques

To evaluate each matrix (A_1 and A_2), we need a numerical or analytical approach for viscosity models. Abou Najm and Atallah (2016) created a Matlab based solver which numerically integrates and optimizes an $N \times N$ matrix to solve the N effective radii of circular pores in a porous medium.

The previous solver is modified in order to account for the planar pore geometries and for the analytical solution of viscosity models, while restricting the number of solutions with $N=2$.

The numerical approach derives the velocity function for Power Law, Cross and Carreau-Yasuda then determines the flow to fill each matrix. However, the analytical approach directly estimates the flow values for Power Law, Cross and Carreau models.

In Sochi 2015, analytical equations are derived for the flow of Carreau and Cross fluids through straight rigid circular uniform pipes and long thin uniform plane slits. The analytical equations (Figure 8) are validated by comparing their solutions to those obtained from numerical integration in Matlab. The comparison show identical results in the investigated case for both Carreau and Cross fluids.

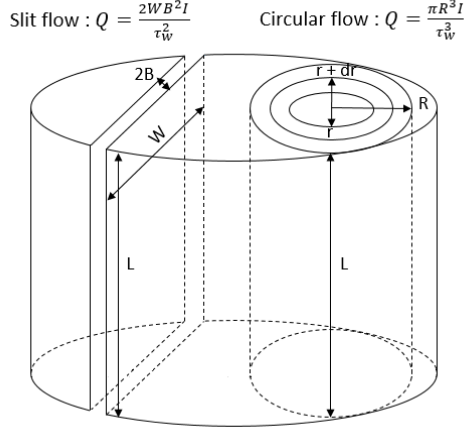


Figure 8: Flow of Carreau and Cross fluids through straight rigid circular uniform pipes and long thin uniform plane slits within the porous medium

D. Problem Types

Similar to the ANA model, ANA-2 solves the derived system of equations to provide answers to three different problem types. A numerical solver was developed for ANA-2 using Matlab optimizer (available upon request from the corresponding author). The solver numerically evaluates the ANA-2 system of equations for a dual-domain soil to answer the following three problem types:

- **Problem-Type 1:** Assuming a relatively known or predefined structure represented as micropores of radius R_1 and tortuosity T_{c_1} as well as macropores of either linear cracks of width W_1 and tortuosity T_{l_1} (Configuration 1) or circular pores of radius R_2 and tortuosity T_{c_2} (Configuration 2), what are the corresponding weights or contributions to total saturated flow Q_1 (with water)? The model output is the following weights: $(w_1)_c$ for circular micropores and $(w_1)_l$ or $(w_2)_c$ for macropores with linear or circular

configurations, respectively. In this problem-type, the objective function is to minimize

$$\frac{1}{2} \|Aw - B\|^2 \text{ subject to: } \begin{cases} w_1 + w_2 = 1 \\ w_{min} \leq w_1 \leq 1 \\ w_{min} \leq w_2 \leq 1 \end{cases}$$

- **Problem-Type 2:** Given pre-defined flow regimes (represented by weights $(w_1)_c$ for circular micropores and $(w_1)_l$ or $(w_2)_c$ for macropores), what are the representative pore size dimensions of the micropores and macropores that satisfy the predefined weights for the given soil? Here, the model output is the micropores representative radius R_1 given tortuosity T_{c1} and the linear cracks representative width W_1 (given tortuosity T_{l1} for Configuration 1) or circular macropores representative radius R_2 (given tortuosity T_{c2} for Configuration 2). In this problem-type, the objective function is to minimize

$$Aw - B \text{ subject to: } \begin{cases} 0 < R_1 < R_2 \\ Or \\ 0 < R_1 < W_2 \end{cases}$$

- **Problem-Type 3:** More generally, and given only the total saturated flows from water (Q_1) and the non-Newtonian fluid (Q_2), what is an optimum and representative pore dual structure that can represent the soil sample and what are the corresponding contributions to flow for each of the micro and macropores? The model output is the micropores representative radius R_1 and contribution to flow $(w_1)_c$ as well as W_1 and $(w_1)_l$ or R_2 and $(w_2)_c$ for macropores with linear or circular configurations, respectively. This problem-type is subject to:

$$\begin{cases} \frac{T_2 R_2^2}{T_1 R_1^2} \geq d_{adj} \\ \frac{T_2 R_2^2}{T_1 R_1^2} \leq d_{range} \end{cases} \quad Or \quad \begin{cases} \frac{T_2 W_1 b_1}{T_1 \pi R_1^2} \geq d_{adj} \\ \frac{T_2 W_1 b_1}{T_1 \pi R_1^2} \leq d_{range} \end{cases}$$

where d_{adj} is the minimum ratio between the 2 representative areas of the pore size geometries for both dual-permeability cases; d_{range} the maximum ratio between the largest and smallest pore size areas such that $d_{range} \geq d_{adj}$ and b_1 is the length of linear cracks determined as function of W_1 where $b_1 = aW_1$, given a the length to width ratio.

E. Optimizer Panels

Four panels are inserted in the Matlab optimizer interface:

- **Flow Characteristics:** take as input the 2 corresponding flows generated from the 2 constant head experiments (water and 1 non-Newtonian fluid), the head gradients $\left(\frac{dh}{dz}\right)$ used or recorded in each experiment and the density of the 2 fluids.
- **Viscosity Characteristics:** list the corresponding parameters of the viscosity model for each fluid.
- **Soil Characteristics:** take as input the porosity, total volume and the saturated depth which is equivalent to the depth of the total soil sample.
- **Simulation Characteristics:** validate the input of the three preceding characteristics, allow the selection of flow direction (horizontal or vertical), problem-type, objective function, constraints (w_{min} , d_{adj} and d_{range}) and the starting pore sizes or weights depending of the selected problem-type.

Those four characteristics are displayed in Figure 9, which presents the Matlab optimizer interface.

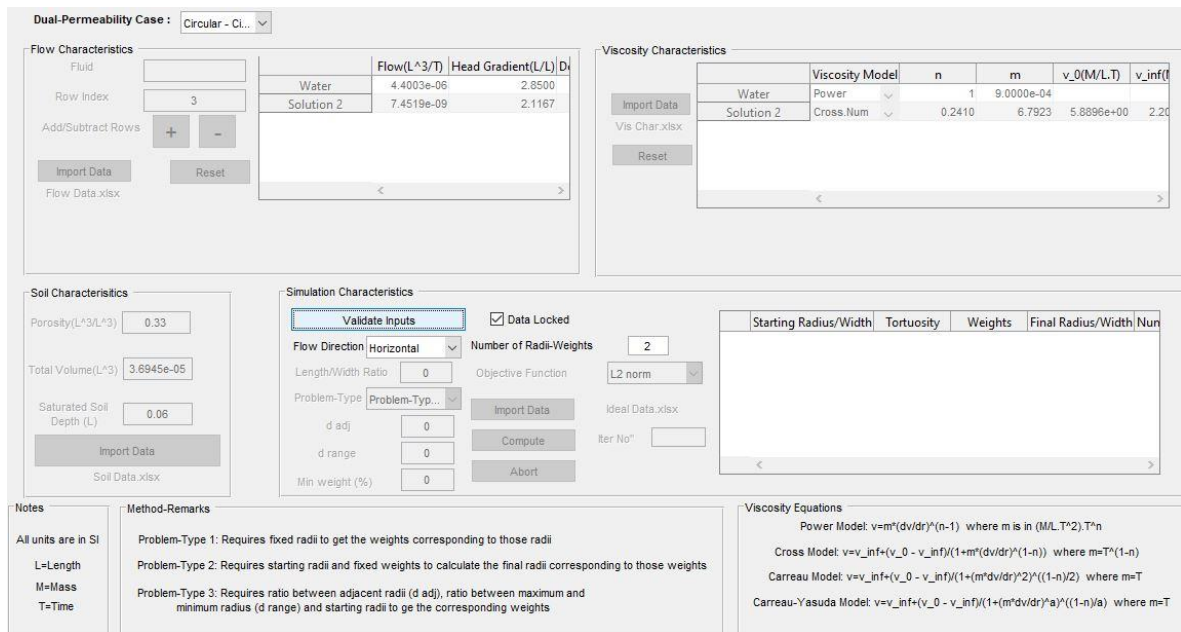


Figure 9: Matlab Optimizer Interface

F. Experimental Validation

We assess the ANA-2 model's ability to identify dual structural characteristics of porous media to aid dual-permeability models in identifying micropore and macropore flow characteristics and dual-permeability model parameters. To achieve this, ANA-2 model predictions were compared with experimental results of engineered dual structures to demonstrate the ANA model's abilities.

1. Experimental Setup

To perform infiltration experiments, a typical Darcy's setup was constructed to accommodate two distinct fluids and the test samples (Figure 10). The system comprised two reservoirs to ensure the two fluids' supply (water and non-Newtonian fluid), a hydraulic pump to maintain constant head, a piezometer to record the head, shutoff and

control valves to adjust the flow and an outlet to collect the fluid once the outflow reaches a steady-state regime.

Soils tested included three standard silica sands representing the matrix flow (micropores) coupled with different numbers of capillary tubes representing preferential flow (macropores). The three silica sands and their corresponding porosities were: #12/20 ($\phi = 0.35$), #20/30 ($\phi = 0.34$), and #40/50 ($\phi = 0.33$). The capillary tubes were inserted vertically along the direction of the flow as one, two or three capillary tubes of 0.75 mm diameter. Infiltration tests were performed in a 50 cm high by 2.8 cm inner diameter tube, in which silica sand was packed to a height of 6 cm. The 6 cm sand columns were supported from the bottom by a mesh fixed to a perforated Plexiglas sheet of 2.7 cm diameter and 1.5 cm thickness, used to sustain the 7.5 cm long, 0.75 mm diameter capillary tubes. This sheet was held by another circular plate of 2.5 cm, perforated at the middle to allow water or non-Newtonian fluids to flow from the pipe into the porous medium. Both sheets were attached with O-rings to restrict drainage. To prepare the soil sample, the following procedure was followed:

First, the capillary tubes of 7.5 cm length were put in place, then sand was poured layer by layer until the 6 cm column is completely covered. Note that the height of the capillary tube was equal to the height of the sand column and the thickness of the Plexiglas sheets. The top surface of the column was similarly covered as its lower inlet. Finally, the outflow fluid mass Δm_j [M] and head [L] were recorded for given interval of time Δt [T] once constant head was reached under saturated conditions. For each fluid, the volumetric flow rate Q_j [L T⁻³] was calculated as $\frac{\Delta m_j}{\rho_j \times \Delta t}$ where ρ_j is the density of fluid [M L⁻³].

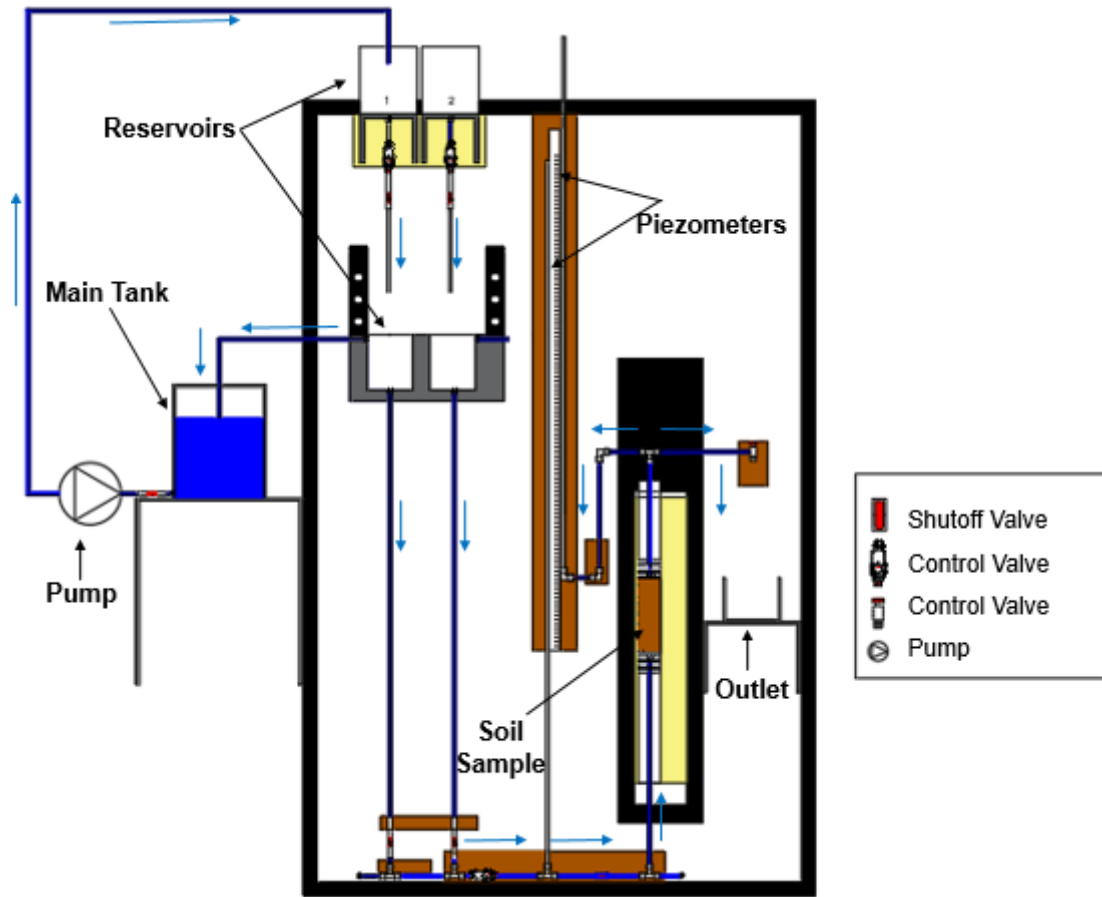


Figure 10: Infiltration Apparatus for Constant Head Experiment

2. *Non-Newtonian Fluid*

For the non-Newtonian fluid, xanthan gum solutions of 0.5 and 1 g/kg (± 0.1 g/kg) concentrations were prepared by combining xanthan gum, deionized water, and sodium azide (0.1% by weight, to prevent biodegradation) in an electric kitchen blender, and blending until xanthan gum was fully dispersed. The mixture was then transferred to a sealed container and stirred with a laboratory electric stirrer for 48h, before being centrifuged for 1h at 2000G and vacuum filtered through a 2.5mm, glass fiber filter. After filtration, the solution was stored in sealed container in the dark at 5 °C. The final

concentration was determined gravimetrically by evaporating an accurately weighed mass of the solution at 105 °C. The Power Law viscosity model ($\eta = k \left(-\frac{\partial v_z}{\partial r} \right)^{\alpha-1}$) parameters for the 0.5 and 1 g kg⁻¹ xanthan gum concentrations were measured with a TA Instruments AR-G2 rotational rheometer with a cone-and-plate configuration. The samples were pre-sheared at 1s⁻¹ for one minute, and then measurements were taken over a torque range of 0.05 to 500Nm at 22C. The apparent viscosity and shear rate values output by the instrument were used to fit the Power law model for each gum solution (Table 2). Both concentrations we tested to emphasize the reliability of the rheological properties of the fluids. Note that both xanthan gum solutions had densities of 1,500 kg m⁻³.

Table 2: Power Law parameters of the two xanthum gum fluids

Concentration (g/kg)	k (Pa.s)	α
0.5	1.2162	0.4269
1	1.8036	0.3638

3. Soil Columns

A total of 21 experiments were conducted including 3 soil configurations and 3 fluids (0.5 and 1.0 g L⁻¹ xanthan gum solutions and water). For the #12/20 and #20/30 silica sands, one, two, and three capillary tubes were used while one capillary tube was used for #40/50 silica sand, making a total of 7 different soil configurations. The experimental saturated flow results from water and each solution of xanthan gum were used as ANA-2 model inputs. For each soil-capillary tube combination, the pore structures of micropores and macropores (obtained from ANA-2 model using water and one non-Newtonian fluid at a time) were compared with results of pore size distributions from 2.5 cm to 3.5 cm soil

sections using a Nikon XTH 225 ST high resolution x-ray microcomputed tomography (μ CT) scanner. The (μ CT) scanning was executed in the Shared Materials Instrumentation Facility (SMIF) at Duke University, with a resolution of between 11.9 to 18.9 μ m/pixel.

4. Dual Pore Structure Calculations

Results from the μ CT showed that the largest pores for the coarsest sand used (#12/20) were less than 0.20 mm, with those of the other two sands (#20/30 and #40/50) having much smaller pores. Thus, the macropores were dominated by the size of the 0.75 mm capillary tubes used, and the micropores were estimated as the average contribution of the entire sand structure. This latter was estimated by discretizing the pore size distribution (assuming all pores are conducting vertically) of each sand into at least 100 pore-size groups per sand type, calculating the number of pores per group from the incremental change in pore volume, and computing the theoretical flow per group using the Hagen-Poiseuille equation to obtain the total theoretical flow, Q [$L^3 T^{-1}$]. Thus, for each soil, the average corresponding pore radius R and number of pores X were estimated using the following system of equations:

$$\begin{cases} Q = X\pi\Delta P R^4 / (8\mu L T) \\ \phi = X\pi R^2 / A_T \end{cases} \quad (30)$$

Then we used the total theoretical flow to back calculate an average micropore size given the total porosity of the sand as follow:

$$\begin{cases} R = \sqrt{(8\mu L T Q) / (\phi A_T \Delta P)} \\ X = (\phi A_T) / (\pi R^2) \end{cases} \quad (31)$$

Figure 11 illustrates the pore size distribution of each of the three silica sands (#12/20, #20/30, and #40/50) while highlighting the average corresponding pore radius previously defined. In order to assess the performance of the infiltration apparatus, we plotted simultaneously the average pore radius calculated from experimental results of saturated water flow through each type of sand, satisfying our presumption in the several different porous sands.

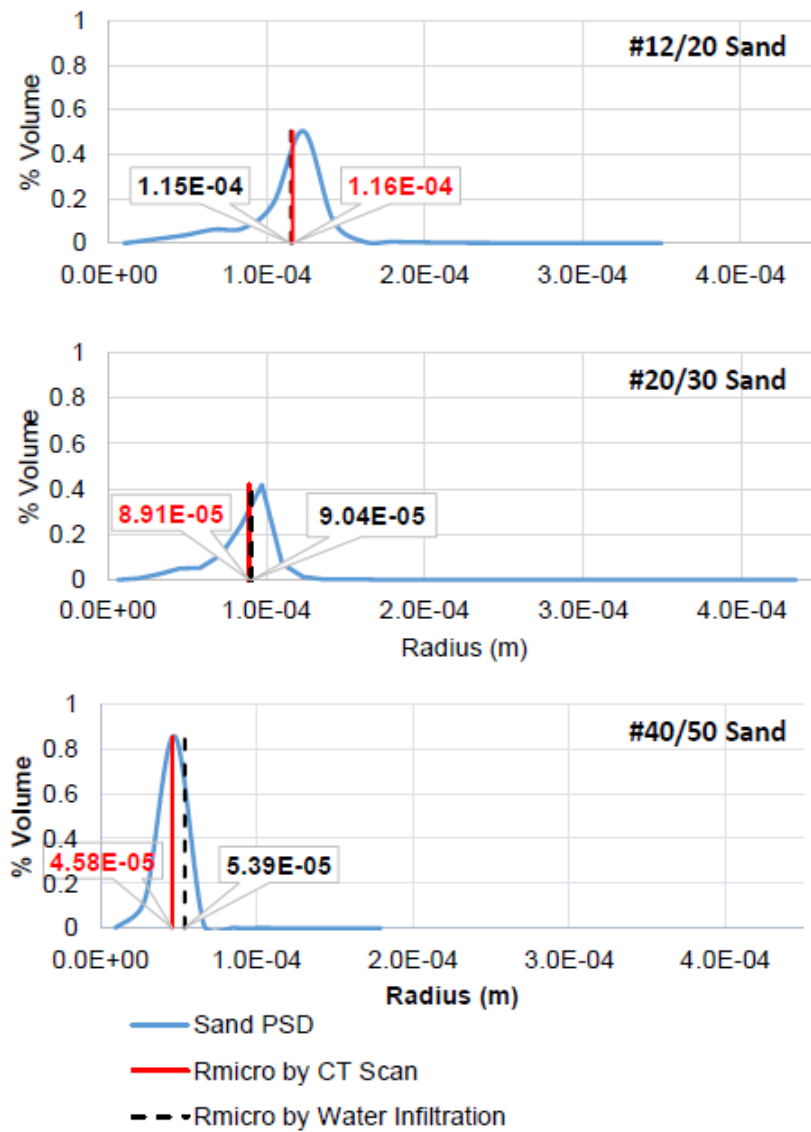


Figure 11: Pore size distribution of each of the three silica sands

The macropore (0.75mm) and each micropore size plotted in Figure 11 (hereafter referred to as experimental radii) were used to validate the ANA-2 macropore and micropore size estimates. The weights or contributions to flow were also calculated from the experimental results of total saturated water flow (Q_1) for each soil combination (sand plus M capillary tubes) by assuming that total flow (Q_1) is equal to the sum of flow from the sand plus the capillary tubes, and realizing that the flow in the macropores (0.75 mm radius capillary tubes) can be calculated from the Hagen-Poiseuille equation. The resulting weights w_1 and w_2 (for micropores and macropores, respectively) add up to 1 and hereafter are referred to as experimental weights.

CHAPTER III

RESULTS AND DISCUSSION

Experimental flows for water (Q_1) and xanthan gum fluid (Q_2) were used to solve the different optimization problems under the three problem-types. In Problem-Type 1, the model was provided with the experimental radii of the two dominant porous structures (sand and capillary tubes) to solve for the corresponding weights (w_{macro}) and (w_{micro}) or contributing to flow of macropores and micropores. In Problem-Type 2, the model was provided with the experimental weights to solve for the corresponding radii (R_{macro}) and (R_{micro}) of macropores and micropores. In Problem-Type 3, the corresponding radii and weights of the macropores and micropores were obtained without any help to the model. Results from the seven soil combinations under the three different problem types were used to evaluate the ANA-2 model ability to physically extract pore structural information that can be used in parameterizing dual-permeability models, using non-Newtonian fluids.

A. Model Predictions under Problem Type 1

Table 3 summarizes the results of the simulations for all three sands and seven soil combinations (sand with one, two or three capillary tubes) at different tortuosities under Problem-Type 1. The weights (flow contributions) were obtained by the ANA-2 model given the experimental average pore radii representing the micropores and the macropores. Statistical differences between experimental and modeled weights were between 1-7% when each of the two pore structures contributed to at least 10% of the total flow. The model was not able to capture the micropores contribution when macropores dominated the

total flow (> 90%), leaving micropores with small contributions of 1 and 2% (in the cases of #20/30 sand with three capillary tubes and #40/50 with one capillary tube, respectively). However, the model captured correctly the macropores contributions of those two cases, with only 5 and 4% differences between modeled and experimentally calculated weights.

Table 3: Problem-Type 1 Summary

Problem-Type 1								
Type of Sand	Number of Macropores M	Tortuosity of Sand (Between 1.2 and 3)	Weights (%) by ANA-2 Model		Experimental Weights (%)		Statistical Difference*	
			W _{micro}	W _{macro}	W _{micro}	W _{macro}	Diff _{micro}	Diff _{macro}
#12/20	M=1	1.224	64%	36%	67%	33%	-0.03	0.07
	M=2	1.402	42%	58%	43%	57%	-0.03	0.02
	M=3	1.807	22%	78%	23%	77%	-0.03	0.01
#20/30	M=1	1.227	51%	49%	50%	50%	0.016	-0.02
	M=2	1.810	20%	80%	19%	81%	0.040	-0.01
	M=3	3.000	6%	94%	1%	99%	4.023	-0.05
#40/50	M=1	3.000	5%	95%	2%	98%	2.333	-0.04

*Statistical Difference = (Modeled – Experimental) / Experimental

B. Model Predictions under Problem Type 2

The ANA-2 model was next used to simulate the flow results under Problem Type (Figure 12). Here, experimental weights were provided and macropores were given a tortuosity of 1 while a wide range of hydraulic tortuosity models (Table 1) was tested for the micropores leading to tortuosity values ranging from 1.2 to 3. To highlight the contribution to flow, Figure 12 plots the % flow vs. pore size in an attempt to show the large contribution to flow from macropores (33-98% of total flow) despite the fact that they all contributed less than 1% of total pore space in the three cases. Furthermore, the porosity and volumetric contribution of micropores and macropores are highlighted on each graph

by two circles showing the corresponding % volume of the micropores and macropores in order to emphasize the micro and macro contribution to the total porosity.

Comparisons between modeled and experimental radii reveal the model's ability to estimate the effective pore sizes of the dual structure. The model accurately estimated the 0.75 mm radius of the capillary tube for the three dual soil configurations. Moreover, the model captured correctly the actual micropore radius of the #12/20 and #20/30 sand, with only 1 and 5% differences between modeled and experimental sizes respectively. However, the model was not able to capture the micropore size when macropores dominated the total flow (> 90% in the case #40/50 sand), leading to under-estimations in the micropore size estimate.

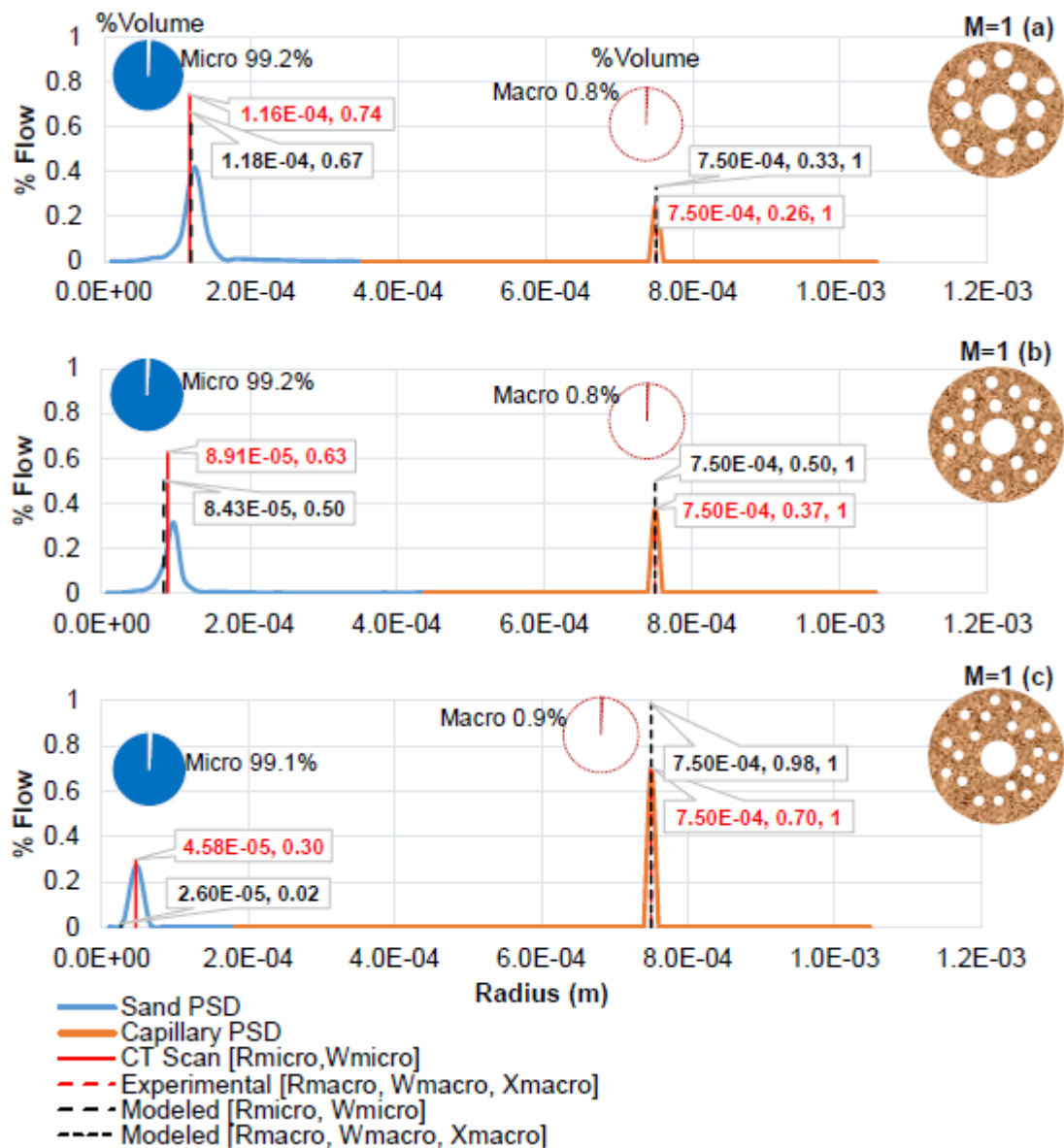


Figure 12: Bimodal pore size distribution in the dual-domain structure built with one capillary tube of 0.75 mm radius along with the #12/20 (a) of tortuosity $T=1.2$, #20/30 (b) of $T=1.2$ and #40/50 (c) of $T=3$. Experimental results highlighted in red representing the porous structure in two points (R_{micro}, W_{micro}) and (R_{macro}, W_{macro}). Similarly, the two simulated radii predicted by the ANA model highlighted in black with the pre-defined set of weights estimated experimentally using the Hagen-Poiseuille equation.

However, as the number of capillary tubes increased from only one tube to 2 or 3 tubes, the model's ability to provide an accurate estimate of the macropores radii size was reduced. This is demonstrated in Figure 13, which shows model estimates for the #12/20 and #20/30 silica soils with two and three capillary tubes. The #40/50 sand experiment with two and three capillary tubes was disregarded since macropores dominated flow with 98% contribution to flow with only one 0.75 mm tube. In all cases, the model assumed that the macropore domain was composed of a single pore, thus not identifying experiments where the soil had two or three capillary tubes. In those instances, the model estimated a larger pore size to match the assigned weights needed for the macropore contribution to flow. Still, the model is simulating a similar hydraulic behavior as the real soil, with the same relative contributions of the micropore and macropore domains to total flow, at slightly smaller %volume or porosity for macropores (Table 4).

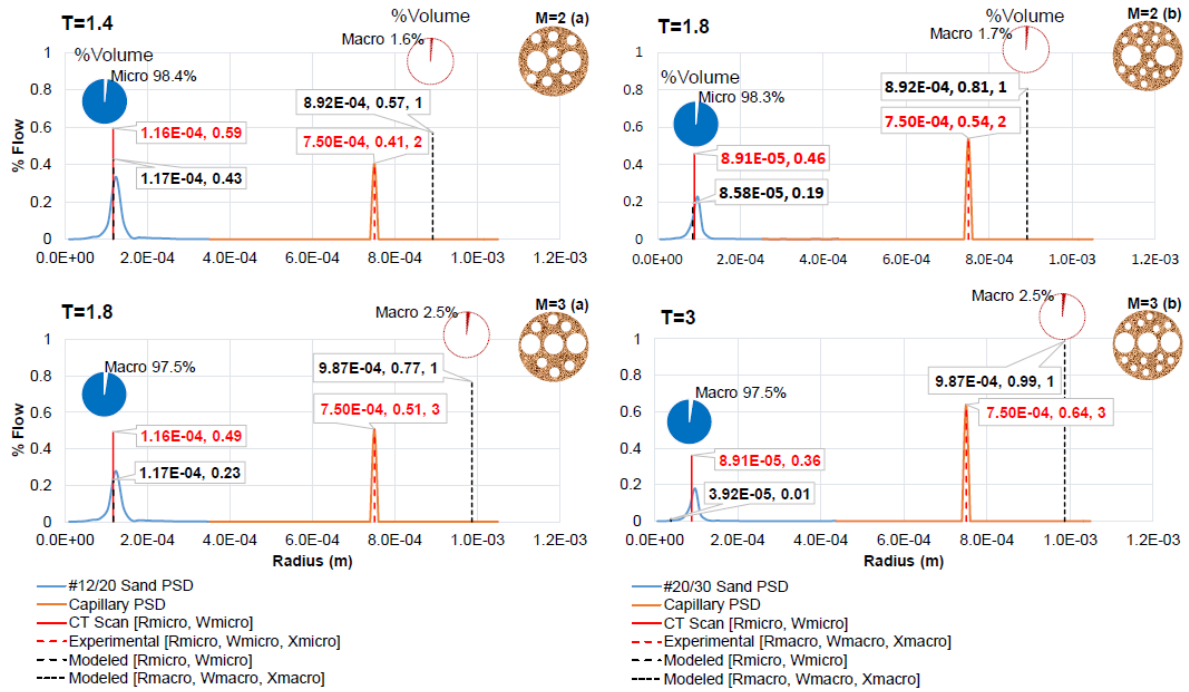


Figure 13: Bimodal pore size distribution in the dual-domain structure built with one and two and capillary tubes of 0.75 mm radius with #12/20 (a) and #20/30 (b) silica sand

Table 4: Problem Type 2 Summary

Macropores Characterization	M=1		M=2		M=3	
	Experiment	ANA model	Experiment	ANA model	Experiment	ANA model
$R_{macro} (m)$	7.50E-04	7.50E-04	7.50E-04	8.92E-04	7.50E-04	9.87E-04
X_{macro}	1	1	2	1	3	1
$K_{macro} (m/s)^*$	2.20E-03	2.20E-03	4.40E-03	4.40E-03	6.60E-03	6.60E-03
Sand Type 1	#12/20 Sand					
% Volume **	0.82%	0.82%	1.65%	1.16%	2.47%	1.43%
Sand Type 2	#20/30 Sand					
% Volume	0.84%	0.84%	1.65%	1.16%	2.51%	1.43%
Sand Type 3	#40/50 Sand					
% Volume	0.87%	0.87%				
$* K = \frac{\pi \rho g X R^4}{8 \mu A_T}$; $** \%Volume = \frac{\pi X R^2}{\phi A_T}$						

C. Model Predictions under Problem Type 3

While Problem Types 1 and 2 generate unique solutions, there is no unique solution under Problem Type 3, which solves two equations with four unknowns (radii R_{micro} and R_{macro} and their corresponding weights w_{micro} and w_{macro}) that vary simultaneously. Therefore, we investigated the stability of the obtained solutions to check whether they remain within acceptable margins from the experimental results for a wide range of runs and starting points. Thus, we performed 25 runs on each scenario from different and randomly selected starting points. The results of flow and pore structure predicted under Problem Type 3 were clustered around the experimental flow contributions and radii of macro and micro pores for the three dual structures soil combinations. (Figure 14).

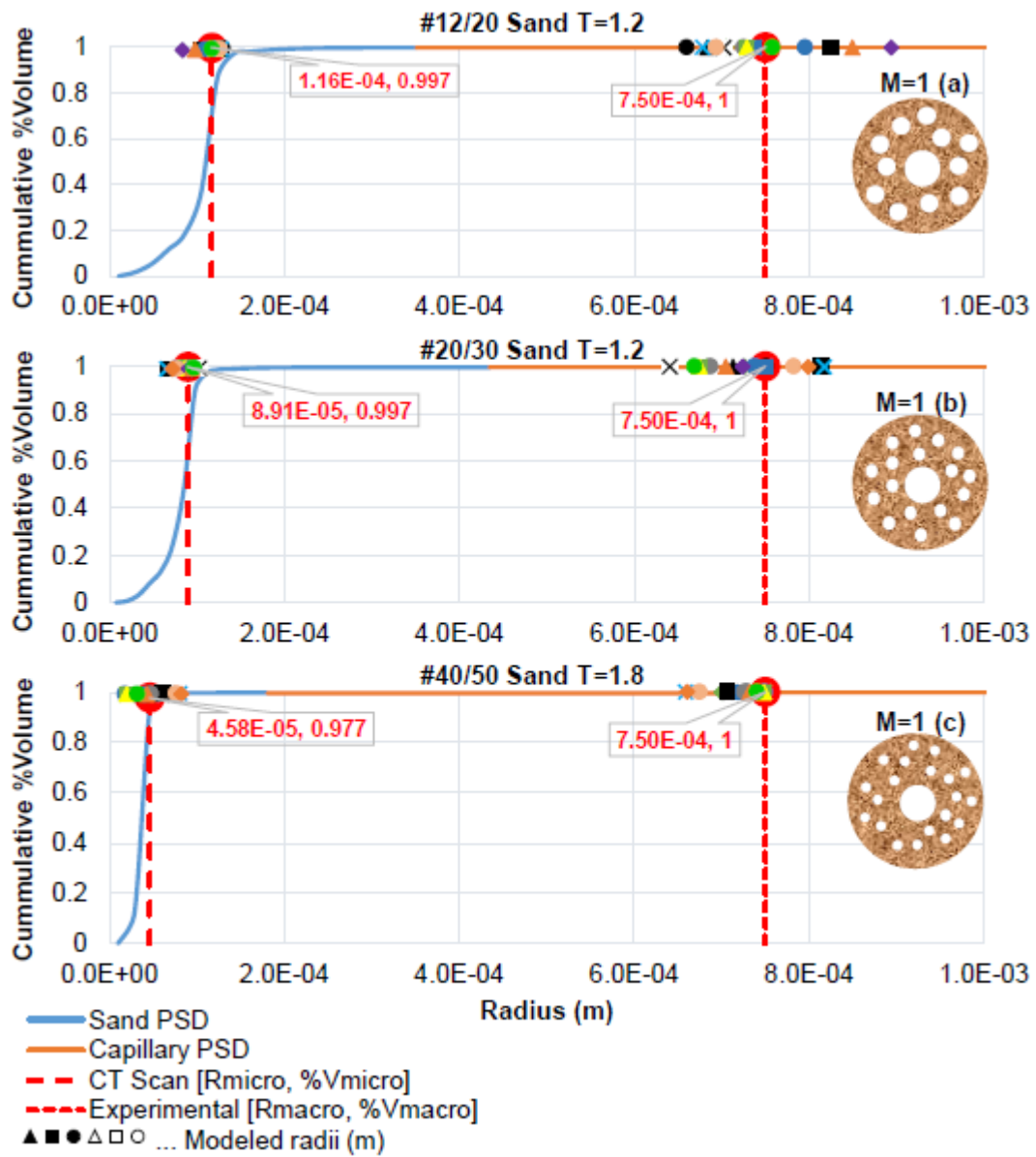


Figure 14: Cumulative pore size distribution of the dual-domain structure built with one capillary tube of 0.75 mm radius with #12/20 (a), #20/30 (b) and #40/50 silica sand. Red circles signifying the experimental averaged micropore radius and corresponding weight (R_{micro} , $\%V_{micro}$) as well as the experimental (actual) macropore radius and its corresponding weight and numbers (R_{macro} , $\%V_{macro}$). Results of the 25 ANA-2 model runs plotted through a wide array of symbols.

As the number of capillary tubes increased from one tube to two or three tubes, the ANA-2 model was constantly capable of solving Problem Type 3 with representative radii of micropores clustered around the radii of the actual pores (Figure 15). However, the model predicted the macropore structure with providing possible solutions of the larger macropore radius with relatively smaller numbers. It is worth noting that both structures were hydrologically equivalent for all the soils tested. This behavior was previously encountered in the Problem Type 2 analysis, which emphasizes the consistency in results of the ANA-2 model between the different optimization problems.

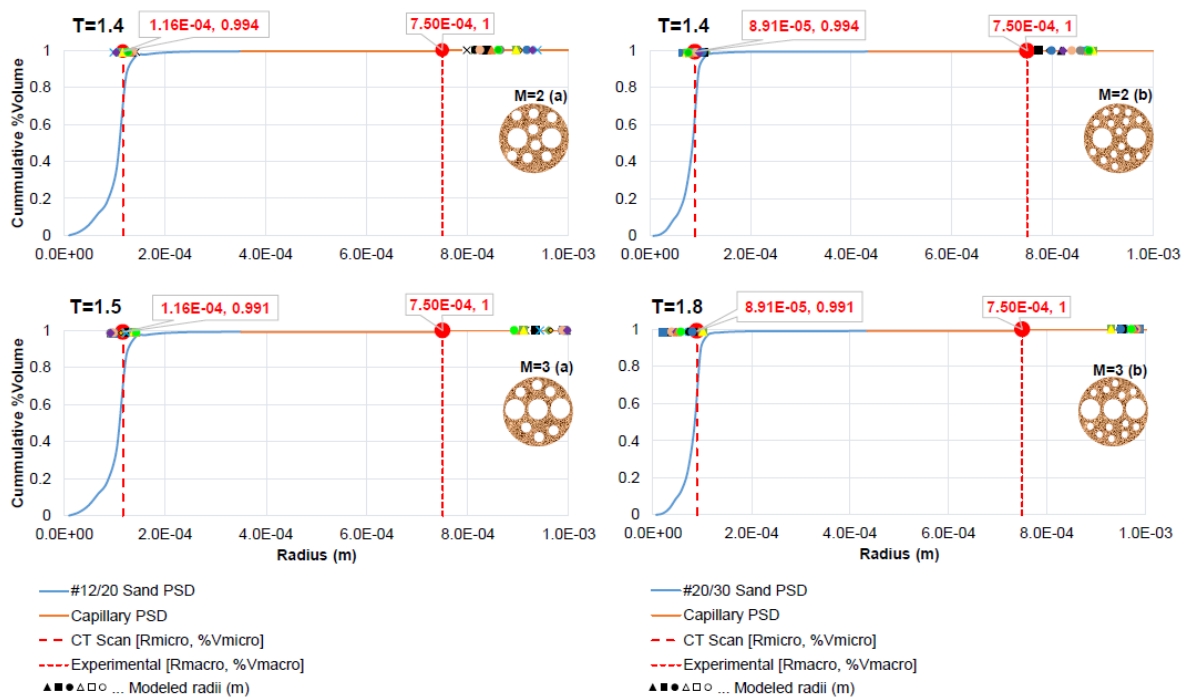


Figure 15: Cumulative pore size distribution of the dual-domain structure built with one and two and capillary tubes of 0.75 mm radius with #12/20 (a) and #20/30 (b) silica sand

Despite the infinite theoretical number of solutions, the ANA model provides an effective characterization of the pore structure under Problem Type 3 (Table 5).

Table 5: Problem-Type 3 Summary

	M=1		M=2		M=3	
Sand Type 1	#12/20 Sand					
	Experiment	ANA model	Experiment	ANA model	Experiment	ANA model
$R_{\text{micro}} m$	1.16E-04	1.16E-04	1.16E-04	1.16E-04	1.16E-04	1.10E-04
$R_{\text{macro}} m$	7.50E-04	7.59E-04	7.50E-04	8.96E-04	7.50E-04	9.69E-04
X_{macro}	1	1	2	1	3	1
<i>Equivalent</i> $R_{\text{macro}} m$	7.50E-04	7.59E-04	7.50E-04	7.54E-04	7.50E-04	7.36E-04
$w_{\text{micro}} \%$	66.67%	65.11%	42.99%	41.81%	23.13%	28.58%
$w_{\text{macro}} \%$	33.33%	34.89%	57.01%	58.19%	76.87%	71.42%
Sand Type 2	#20/30 Sand					
	Experiment	ANA model	Experiment	ANA model	Experiment	ANA model
$R_{\text{micro}} m$	8.91E-05	8.45E-05	8.91E-05	7.88E-05	8.91E-05	2.38E-05
$R_{\text{macro}} m$	7.50E-04	7.49E-04	7.50E-04	8.70E-04	7.50E-04	9.87E-04
X_{macro}	1	1	2	1	3	1
<i>Equivalent</i> $R_{\text{macro}} m$	7.50E-04	7.49E-04	7.50E-04	7.31E-04	7.50E-04	7.50E-04
$w_{\text{micro}} \%$	50.13%	50.40%	19.27%	27.08%	1.19%	1.21%
$w_{\text{macro}} \%$	49.87%	49.60%	80.73%	72.92%	98.81%	98.79%
Sand Type 3	#40/50 Sand					
	Experiment	ANA model				
$R_{\text{micro}} m$	4.58E-05	1.96E-05				
$R_{\text{macro}} m$	7.50E-04	7.48E-04				
X_{macro}	1	1				
<i>Equivalent</i> $R_{\text{macro}} m$	7.50E-04	7.48E-04				
$w_{\text{micro}} \%$	1.50%	2.31%				
$w_{\text{macro}} \%$	98.50%	97.69%				

D. Summary of results

Overall, the ANA-2 model was capable of predicting the micropores and macropores flow characteristics of dual structured soils given only the total flows from water and one non-Newtonian fluid. This effectiveness was demonstrated by the results under Problem Type 1 (Table 3) where the ANA-2 model was capable of predicting the flow contributions (weights of macro and micro structures) compared to the weights estimated using the Hagen-Poiseuille equation. A similar conclusion can be inferred from the model's estimation of the pore structure of the dual structured soils under Problem Type 2, particularly when one capillary tube was used (Figure 12). In addition, the ANA-2 model provides an effective characterization of the same dual soil configuration (i.e. $M=1$) under Problem Type 3 analysis despite the infinite theoretical number of solutions (Figure 14). However, the model was less successful in predicting the macropore structure when more than one capillary tube was used (Figure 13 and Figure 15), though it still provided a satisfactory simulation for flow distributions between domains. We should mention that the two concentrations of xanthan gum solutions (0.5 and 1.0 g/L) were analyzed under the three problem types. The rheological properties provide similar results in all scenarios, which emphasizes the well-posedness of the rheological data as well as the efficiency of the experimental procedures.

CHAPTER IV

CONCLUSION

This study developed a new physically based model to extract dual-permeability parameters from heterogeneous soils using non-Newtonian fluids. Due to the complexity of the pore structure, this latter is characterized by two effective pore sizes, one for the macropores of either cylindrical (e.g., biological pores) or planar (e.g., shrinkage cracks and fissures) pore geometries of high permeability, and one for the circular micropores of low permeability. This method utilizes two solutions including water and one non-Newtonian fluid to predict the two representative circular pore sizes and their corresponding contributions (weights) to total water flow. The efficiency of the proposed method was validated through a sequence of infiltration experiments with porous dual-domain samples made out of silica sand (as the micropore domain) and different numbers of capillary tubes (as the macropore domain). Results illustrated the ability of the model to characterize and quantify the representative macro and micro pores using only flows generated from two saturated infiltration experiments.

This study introduces the use of non-Newtonian fluids for dual-permeability characterization using a relatively cheap and simple method, requiring limited input and simple experimental procedures. It is worth noting that the model did not perform as effectively when macropores dominated the flow, rendering this a point of further investigation. For example, when macropores dominated the flow, as occurred when more macropores were added to the soils, the model under-predicted the average micropore size. This result can be explained by the high contribution of macropores to water flow (beyond

90%), in which most of the water flows through the highly conducting macropores while acting insensitive to a large part of the micropores. At this level, the hydraulic conductivity of the matrix (micropores) becomes negligible compared to that of the macropores, and the system tends to behave as single porosity/permeability domain.

Many different adaptations, tests, and experiments have been left for the future due to the time constraint. Future work concerns further assessment of the ANA-2 model's ability to identify dual structural characteristics of porous media composed of circular micropores and linear cracks. This can be achieved using the water infiltration apparatus, where soils representing the matrix flow (micropores) can be tested with different numbers of capillary tubes of rectangular cross section representing the linear cracks. Obviously, the use of other experimental techniques can be investigated to improve our preliminary results and acquire better understanding of the preferential flow processes. It can be interesting to consider the injection of water and 1 non-Newtonian fluid into real macroporous soils as a transition from an infiltration dominated flow regime to a fracturing dominated regime.

APPENDIX

A. Detailed Derivations

The derivations for the velocity profile in the special cases of non-Newtonian power law viscosity model and water are as follows:

$$\frac{d}{dy} \left(\beta \left(-\frac{du}{dy} \right)^{\alpha-1} \left(\frac{du}{dy} \right) \right) = \frac{H_j}{T_i} \quad (32)$$

where j the number of fluids and i the number of representative geometries.

$$\frac{d}{dy} \left(\beta (-1)^{\alpha-1} \left(\frac{du}{dy} \right)^\alpha \right) = \frac{H_j}{T_i} \quad (33)$$

$$\beta (-1)^{\alpha-1} \left(\frac{du}{dy} \right)^\alpha = \frac{H_j}{T_i} y + c_1 \quad (34)$$

$$\left((-1)^{\alpha-1} \left(\frac{du}{dy} \right)^\alpha \right)^{\frac{1}{\alpha}} = \left(\frac{1}{\beta} \frac{H_j}{T_i} y + c_1 \right)^{\frac{1}{\alpha}} \quad (35)$$

$$(-1)^{\frac{\alpha-1}{\alpha}} \left(\frac{du}{dy} \right) = \left(\frac{1}{\beta} \frac{H_j}{T_i} y + c_1 \right)^{\frac{1}{\alpha}} \quad (36)$$

For $y = 0, \frac{du}{dy} = 0 \rightarrow c_1 = 0$

$$(-1)^{\frac{\alpha-1}{\alpha}} \left(\frac{du}{dy} \right) = \left(\frac{H_j}{\beta T_i} \right)^{\frac{1}{\alpha}} y^{\frac{1}{\alpha}} \quad (37)$$

$$(-1)^{\frac{\alpha-1}{\alpha}} u = \frac{\alpha}{\alpha+1} \left(\frac{H_j}{\beta T_i} \right)^{\frac{1}{\alpha}} y^{\frac{1}{\alpha}+1} + c_2 \quad (38)$$

For $y = +W/2, u = 0$ (no slip boundary condition)

$$\rightarrow c_2 = -\frac{\alpha}{(\alpha+1)2^{\frac{1}{\alpha}+1}} \left(\frac{H_j}{\beta T_i} \right)^{\frac{1}{\alpha}} W^{\frac{1}{\alpha}+1} \quad (39)$$

where $W(L)$ the distance between the two parallel fixed plates (i.e. the width)

$$(-1)^{\frac{\alpha-1}{\alpha}} u = \frac{\alpha}{\alpha+1} \left(\frac{H_j}{\beta} \frac{1}{T_i} \right)^{\frac{1}{\alpha}} y^{\frac{1}{\alpha}+1} - \frac{\alpha}{(\alpha+1)2^{\frac{1}{\alpha}+1}} \left(\frac{H_j}{\beta} \frac{1}{T_i} \right)^{\frac{1}{\alpha}} W^{\frac{1}{\alpha}+1} \quad (40)$$

Multiply each term by $(-1)^{\frac{1}{\alpha}}$

$$-u = \frac{\alpha}{\alpha+1} \left(-\frac{H_j}{\beta} \frac{1}{T_i} \right)^{\frac{1}{\alpha}} y^{\frac{1}{\alpha}+1} - \frac{\alpha}{(\alpha+1)2^{\frac{1}{\alpha}+1}} \left(-\frac{H_j}{\beta} \frac{1}{T_i} \right)^{\frac{1}{\alpha}} W^{\frac{1}{\alpha}+1} \quad (41)$$

$$u = \frac{\alpha}{\alpha+1} \left(-\frac{H_j}{\beta} \frac{1}{T_i} \right)^{\frac{1}{\alpha}} \left\{ \frac{1}{2^{\frac{1}{\alpha}+1}} W^{\frac{1}{\alpha}+1} - y^{\frac{1}{\alpha}+1} \right\} \quad (42)$$

In the case of Newtonian fluids, $\alpha = 1$; therefore, the velocity of water, u_{water} , is found

by:

$$u_{water} = \frac{1}{2} \left(-\frac{H_1}{\mu} \frac{1}{T_i} \right) \left\{ \frac{1}{4} W^2 - y^2 \right\} \quad (43)$$

where μ is the viscosity of water in (P T).

The volume rate of flow for a unit length is obtained from the relationship:

$$q = \int_{-W/2}^{W/2} u dy = \frac{\alpha}{\alpha+1} \left(-\frac{H_j}{\beta} \frac{1}{T_i} \right)^{\frac{1}{\alpha}} \left[\int_{-W/2}^{W/2} \left(\frac{1}{2^{\frac{1}{\alpha}+1}} W^{\frac{1}{\alpha}+1} - y^{\frac{1}{\alpha}+1} \right) dy \right] \quad (44)$$

where:

$$\begin{aligned} \int_{-W/2}^{W/2} \left(\frac{1}{2^{\frac{1}{\alpha}+1}} W^{\frac{1}{\alpha}+1} - y^{\frac{1}{\alpha}+1} \right) dy &= 2 \times \int_0^{W/2} \left(\frac{1}{2^{\frac{1}{\alpha}+1}} W^{\frac{1}{\alpha}+1} - y^{\frac{1}{\alpha}+1} \right) dy \\ &= 2 \times \left[\left(\frac{1}{2^{\frac{1}{\alpha}+1}} W^{\frac{1}{\alpha}+1} y \right) - \frac{\alpha}{2\alpha+1} \left(y^{\frac{1}{\alpha}+2} \right) \right] \Bigg|_0^{W/2} \\ &= 2 \times \left[\frac{1}{2^{\frac{1}{\alpha}+2}} W^{\frac{1}{\alpha}+2} - \frac{\alpha}{(2\alpha+1)2^{\frac{1}{\alpha}+2}} \left(W^{\frac{1}{\alpha}+2} \right) \right] \\ &= \left[\frac{\alpha+1}{(2\alpha+1)2^{\frac{1}{\alpha}+1}} \right] \left(W^{\frac{1}{\alpha}+2} \right) \end{aligned} \quad (45)$$

Then, the flow rate is given by:

$$q = \frac{\alpha}{(2\alpha+1)2^{\frac{1}{\alpha}+1}} \left(-\frac{H_j}{\beta} \frac{1}{T_i} \right)^{\frac{1}{\alpha}} W^{\frac{1}{\alpha}+2} \quad (46)$$

In the case of Newtonian fluids, $\alpha = 1$; therefore, the flow of water, Q_{water} , is found by:

$$q_{water} = \frac{1}{12} \left(-\frac{H_1}{\mu} \frac{1}{T_i} \right) W^3 \quad (47)$$

Ultimately, the analytical equation of flow through parallel plates in the special case of non-Newtonian power law viscosity model is therefore:

$$Q = \frac{\alpha}{(2\alpha+1)2^{\frac{1}{\alpha}+1}} \left(-\frac{H_j}{\beta} \frac{1}{T_i} \right)^{\frac{1}{\alpha}} b W^{\frac{1}{\alpha}+2} \quad (48)$$

where b (L) is the width of the plane normal to the plane (i.e. the length)

B. Experimental Illustrations

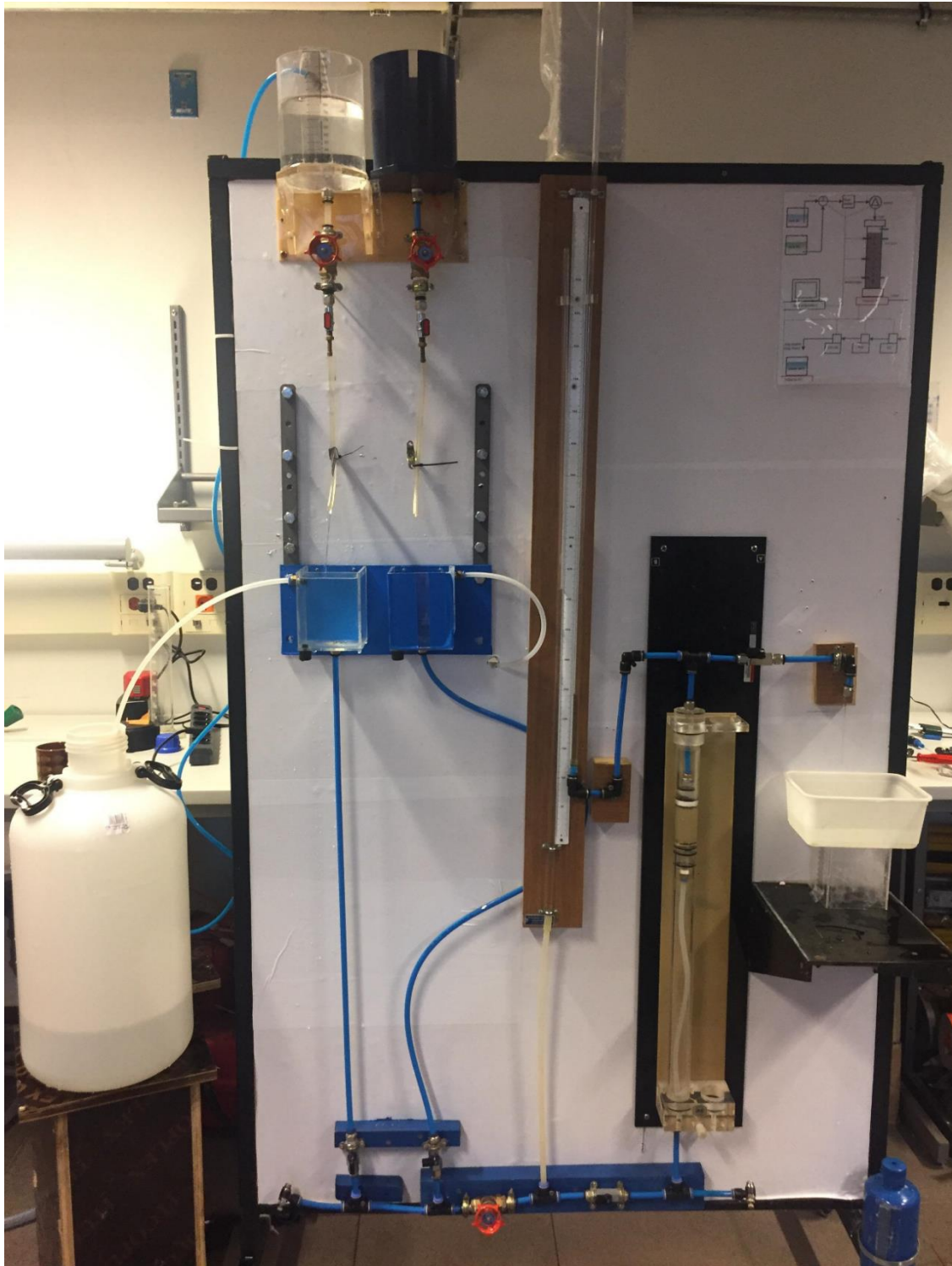


Figure 16: Actual Infiltration Setup for Constant Head Experiment



Figure 17: Different experimental stages



Figure 18: Preparation of xanthan gum fluids

BIBLIOGRAPHY

- Abou Najm, M. R., & Atallah, N. M. (2016). Non-Newtonian Fluids in Action: Revisiting Hydraulic Conductivity and Pore Size Distribution of Porous Media,. *Vadose Zone J.* 15. doi:10.2136/vzj2015.06.0092.
- Abou Najm, M. R., Jabro, J. D., Iversen, W. M., Mohtar, R. H., & Evans, R. G. (2010). New method for the characterization of three-dimensional preferential flow paths in the field,. *Water Resour. Res.* 46(2). doi:10.1029/2009WR008594.
- Ahmadi, M. M., Mohammadi, S., & Hayati, A. N. (2011). Analytical derivation of tortuosity and permeability of monosized spheres: a volume averaging approach. *Phys. Rev. E* 83.
- Archie, G. E. (1942). The electrical resistivity log as an aid in determining some reservoir characteristics. *Metall. Pet. Eng.* 146.
- Atallah, N. M., & Majdi, A. R. (2018 (In review)). Non-Newtonian fluids in Action: An experimental validation for pore structure characterization. *Eur J Soil Sci.*
- Beekman, J. W. (1990). Mathematical description of heterogeneous materials. *Chem. Eng. Sci.* 45(8), 2603-2610.
- Berryman, J. G. (1981). Elastic wave propagation in fluid-saturated porous media. *J. Acoust. Soc. Am.* 69. doi: 10.1121/1.385457.
- Beven, K. J. (1991). Modeling preferential flow: An uncertain future? *American Society of Agricultural Engineers*, 1-11.
- Beven, K., & Germann, P. (1982). Macropores and water flow in soils. *Water Resour. Res.* 18, 1311-1325.
- Boudreau, B. P. (1996). The diffusive tortuosity of fine-grained unlithified sediments. *Geochim. Cosmochim. Acta.* 60(16), 3139-3142.
- Boving, T. B., & Grathwohl, P. (2001). Tracer diffusion coefficients in sedimentary rocks: correlation to porosity and hydraulic conductivity. *J. Contam. Hydrol.* 53, 85-100.
- Bruggeman, D. G. (1935). Calculation of different physical constants of heterogeneous substances. Part I: Dielectric constant and conductivity of media of isotropic substances. *Ann. Phys.* 24, 636-664.
- Carey, G. R., McBean, E. A., & Feenstra, S. (2016). Estimating tortuosity coefficients based on hydraulic conductivity. *Groundwater* 54(4), 476-487.
- Carman, P. C. (1937). Fluid through granular beds. *Trans. Inst. chem. Eng.* 15.

- Comba, S., Dalmazzo, D., Santagata, E., & Sethi, R. (2011). Rheological characterization of xanthan suspensions of nanoscale iron injection in porous media. *J. Hazard. Mater.* 185. doi:10.1016/j.jhazmat.2010.09.060, 598-605.
- Di Federico, V., Pinelli, M., & Ugarelli, R. (2010). Estimates of effective permeability for non-Newtonian fluid flow in randomly heterogenous porous media. *Stochastic Environ. Res. Risk Assess.* 24(7). doi:10.1007/s00477-010-0397-9, 1067-1076.
- Douglas, J., Peszynska, M., & Showalter, R. (1997). Single phase flow in partially fissured media. *Transp. Porous Media*, 278.
- Du Plessis, J. P., & Masliyah, J. H. (1991). Flow through isotropic granular porous media. *Transp. Porous Media* 6(3), 207-221.
- Duda, A., Koza, Z., & Matyka, M. (2011). Hydraulic tortuosity in arbitrary porous media flow. *Phys. Rev. E* 84. doi:10.1103/PhysRevE.84.036319.
- Dullien, F. L. (1975). Single phase flow through porous media and pore structure. *Chem. Eng. J.* 10, 1-34.
- Gastone, F., Tosco, T., & Sethi, R. (2014). Guar gum solutions for improved delivery of iron particles in porous media (Part 1): Porous medium rheology and guar gum-induced clogging. *J. Contam. Hydrol.* 166. doi:10.1016/j.jconhyd.2014.06.013, 23-33.
- Gerke, H. H., & van Genuchten, M. T. (1993a). A dual-porosity model for simulating the preferential movement of water and solutes in structured porous media. *Water Resour. Res.* 29, 305-319.
- Jarvis, N. J. (1994). The MACRO model ver. 3.1: Technical description and sample simulations . *Rep. Diss. 19, Dep of Soil Sci., Swed. Univ. of Agric. Sci., Uppsala.*
- Javis, N. J. (2007). A review of non-equilibrium water flow and solute transport in soil macropores: principles, controlling factors and consequences for water quality. *Eur. J. Soil Sci.* 58(3). doi:10.1111/j.1365-2389.2007.00915.x, 523-546.
- Kohne, J. M., Kohne, S., & Gerke, H. (2002). Estimating the hydraulic functions of dual-permeability models from bulk soil data. *Water Resour. Res.* 38(7). doi:10.1029/2001WR000492.
- Lanfrey, P. Y., Kuzeljevic, Z. V., & Dudukovic, M. P. (2010). Tortuosity model for fixed beds randomly packed with identical particles . *Chem. Eng. Sci.* 65, 1891-1896.
- Larsson, M. H., & Jarvis, N. J. (1999a). Evaluation of a dual-porosity model to predict field-scale solute transport in a macroporous soil. *J. Hydrol.* 215, 153-171.

- Lewandowska, J., Szymkiewicz, A., Burzynski, K., & Vauclin, M. (2004). Modelin of unsaturated water flow in double porosity soils by the homogenization approach. *Adv. Water Resour.* 27(3).
- Li, J. H., & Boming, Y. (2011). Tortuosity of flow paths through a sierpinski carpet. *Chinese Phys. Lett.* 28(3). doi:10.1088/0256-307X/28/3/034701.
- Liu, Y., & Kitanidis, P. K. (2013). A mathematical and computational study of the dispersivity tensor in anisotropic porous media. *Adv. Water Resour.* 62, 303-316.
- Matyka, M., Khalili, A., & Koza, Z. (2008). Tortuosity-porosity realtion in porous media flow. *Phys. Rev. E* 78. doi:10.1103/PhysRevE.78.026306.
- Mauret, E., & Renaud , M. (1997). Transport phenomena in multi-particle systems - I. limits of applicability of capillary model in high voidage beds-application to fixed beds of fibers and fluidized beds of spheres. *Chem. Eng. Sci.* 52(11), 1807-1817.
- Maxwell, J. C. (1881). *Treatise on Electricity and Magnetism, 2nd ed.* Oxford, UK: Clarendon Press.
- Millington, R. J., & Quirk, J. P. (1961). Permeability of porous solids. *Trans. Faraday Soc.* 57, 1200-1207.
- Moldrup, P., Olesen, T., Komatsu, T., Schjonning, P., & Rolston, D. E. (2001). Tortuosity, diffusivity and permeability in the soil liquid and gaseous phases. *Soil Sci. Soc. Am. J.* 65(3), 613-623.
- Mota, M., Teixeira, J. A., Bowen, W. R., & Yelshin, A. (2001). Binary spherical particle mixed bed: porosity and permeability relationship measurement . *Trans. Filt. Soc.* 1(4), 101-106.
- Pisani, I. (2011). Simple expression for the tortuosity of porous media. *Transp. Porous Med.* 88. doi:10.1007/s11242-011-9734-9, 193-203.
- Sanders, E., Abou Najm, M., Mohtar, R., Kladvko, E., & Schulze, D. (2012). Field method for separating the contribution of surface-connected preferential flow pathways from flow through the soil matrix. *Water Resour. Res.*, 48, W04534, doi: 10.1029/2011WR011103.
- Saomoto, H., & Katagiri, J. (2015). Direct comparison of hydraulic tortuosity and electric tortuosity based on finite element analysis. *Theo. App. Mech. Lett.* 5, 177-180.
- Simunek, J., Jarvis, N. J., van Genuchten, M. T., & Gardenas, A. (2003). Review and comparison of models for describing non-equilibrium and preferential flow and transport in the vadose zone. *J. Hydrol.* 272. doi:10.1016/S0022-1694(02)00252-4, 14-35.
- Sochi, T. (2015). Analytical solutions for the flow of Carreau and Cross fluids in circular pipes and thin slits. *Rheologica Acta.* 54(8). doi: 10.1007/s00397-015-0863-x.

Stewart, R. D., Abou Najm, M. R., Rupp, D. E., & Selker, J. S. (2014). Nondestructive quantification of macropore volume using shear-thinning fluid. *Soil Sci. Soc. Am. J.* 78(2). doi:10.2136/sssaj2013.08.0346.

Tosco, T., Gastone, F., & Sethi, R. (2014). Guan gum solutions for improved delivery of iron particles in porous media (Part 2): Iron transport tests and modeling in radial geometry. *J. Contam. Hydrol.* 166. doi:10.1016/j.jconhyd.2014.06.014, 34-51.

van Genuchten, M. T., & Wierenga, P. J. (1976). Mass transfer studies in sorbing porous media. *Soil Sci. Soc. Am. J.* 40, 473-481.

van Genuchten, M. T., Rolston, D. E., & Germann, P. F. (1990). Transport of water and solutes in macropores. *Geoderma.* 46(1).

Weissberg, H. (1963). Effective diffusion coefficients in porous media. *J. Appl. Phys.* 34, 2636-2639.

Yu, B. M., & Li, J. H. (2004). A geometry model for tortuosity of flow path in porous media. *Chinese Phys. Lett.* 21(8).

Yun, M. J., Yu, B. M., Zhang, B., & Huang, M. T. (2005). A geometry model for tortuosity of streamtubes in porous media with spherical particles. *Chinese Phys. Lett.* 22(6).

